# Submillimeter-wave Ice Cloud Radiometry Channel Selection Study

K. Franklin Evans
University of Colorado, Boulder

September 3, 2003 (revised January 23, 2004)

The results in Tables 7 and 8 and Figures 7 to 23 have been revised after fixing a bug in the Bayesian retrieval code that effectively greatly reduced the retrieval database size. The exact same channel sets and retrieval and testing databases have been used in the revised results. The revised retrieval errors are lower and more reliable, but the conclusions about the relative merits of various channel sets did not change.

## 1. Introduction

Submillimeter-wave remote sensing of ice clouds is a new technique for retrieving ice cloud mass and particle size, which has been developed so far mostly with theoretical work (e.g. Evans et al., 1998). Radiometer measurements at multiple frequencies over the range from 180 to 900 GHz are more directly related to vertically integrated ice mass (or ice water path, IWP) and median volume equivalent sphere particle diameter ($D_{me}$) than other ice cloud remote sensing techniques such as millimeter-wave radar. As such, the submillimeter ice cloud remote sensing technique, in addition to being used to retrieve IWP and $D_{me}$, can be used to test algorithms that retrieve ice cloud mass from radar reflectivity.

Recently, several aircraft submillimeter radiometers have been built, including the Submillimeter-Wave Cloud Ice Radiometer (SWCIR) developed at the Jet Propulsion Laboratory (JPL) (Evans et al., 2002), the Conical Scanning Submillimeter-wave Imaging Radiometer (CoSSIR) developed at NASA's Goddard Space Flight Center, and the Far Infrared Sensor for Cirrus (FIRSC) developed at NASA's Langley Research Center (Vanek et al., 2001). FIRSC flew in a number of experiments from 1998 to 2002, CoSSIR's first deployment (and only to this date) was in the CRYSTAL-FACE experiment in Florida in 2002, and SWCIR has not been flown. FIRSC is a Fourier transform spectrometer with a $^3$He cooled bolometer, while CoSSIR and SWCIR are heterodyne radiometers with room temperature solid state receivers. The heterodyne approach is more promising for space instruments because expensive cryogenic systems are avoided, individual measurements are obtained much more rapidly allowing cross track scanning, and heterodyne radiometers have less noise at the important lower frequencies (say below 600 GHz). The challenges for heterodyne technology are achieving low-noise room-temperature receivers above 600 GHz and reducing the mass and power, and hence cost, of a multifrequency space instrument. Submillimeter heterodyne radiometers have been (or will be) flown in space for astronomy (SWAS and Odin) and atmospheric

chemistry (Odin and EOS Microwave Limb Sounder to be launched in 2004). Space missions have been proposed to measure the climatology of ice cloud mass and particle size, with the most recent proposal being the Cloud Ice and Water-vapor Sub-mm Imaging Radiometer (CIWSIR, Miao et al., 2002). With new submillimeter-wave aircraft instruments under developement and space instruments being proposed, it would be useful to determine the best set of frequencies to use. While the submillimeter cirrus retrieval simulation technology developed in Evans et al. (2002) has been applied in limited ways to SWCIR and CIWSIR, it has never been used to study the more general issue of the optimal frequencies for submillimeter remote sensing of ice clouds.

This report describes an in depth study of the theoretical retrieval accuracy of ice cloud properties and water vapor profiles with many different microwave frequency configurations. Retrieval simulations are performed for 44 double sideband microwave frequencies from 183 GHz to 916 GHz and 4 infrared channels centered at 6.7, 8.5, 11.0, and 12.0. Most of the frequency configurations consist of six heterodyne receivers, though the configurations range from three to six microwave receivers and one to four infrared channels. The instrument viewing geometry is a fixed zenith angle of 53° appropriate for a conically scanning geometry. The simulated retrievals estimate the expected accuracy of IWP, $D_{me}$, median IWP cloud height ($Z_{medIWP}$), and water vapor profiles for a wide variety of ice clouds. The simulations are performed for two situations: tropical convective anvils and mid-latitude winter synoptic ice clouds. For each retrieval simulation 10,000 atmospheres are randomly generated with a realistic range of temperature and humidity profiles, ice cloud heights and thicknesses, vertically inhomogeneous IWC and $D_{me}$, ice particle shape (randomly oriented) and size distribution, and mixed phase and lower level water clouds. A radiative transfer model is used to simulate microwave brightness temperatures and infrared radiances from these profiles. Realistic Gaussian noise is added to the observations to simulate instrument and model errors. The simulated observations are input to a Bayesian retrieval algorithm described below, and the resulting retrieved ice cloud IWP, $D_{me}$, and $Z_{medIWP}$ are compared to the true values.

A second part of the report examines the range of polarized radiance that could be expected from different ice crystal types and investigates the retrieval accuracy using vertical and horizontal polarized brightness temperature (Section 7.).

## 2. Candidate Frequencies

A large number of candidate microwave frequencies from 183 to 916 GHz were chosen so that many sets of frequencies could be tested with the retrieval simulations. Most of the frequencies are from sets of double sideband channels on water vapor and oxygen absorption lines. The rationale for this is that one receiver centered on an absorption line can provide several channels with independent information for a relatively small additional cost. The offset frequency from the line center is constrained by the available bandpass of very low noise IF amplifiers, taken here to be 0.5 to 11 GHz. The channels farthest from the absorption line centers are chosen, within this constraint, to have atmospheric transmission characteristics similar to window channels. There are frequencies from all the major absorption lines from 183 to 916 GHz, except for the 557 and 752 GHz water vapor lines, which are too strong for tropospheric use, and two oxygen lines (715 and 774 GHz) near the 752 GHz line. Double sideband channels were also selected for window regions between lines. The frequencies of these channels were chosen based on their use in previous proposals (e.g. CIWSIR), for being on existing aircraft radiometers (e.g. CoSSIR and SWCIR), or

Table 1: Frequencies of 44 Microwave Channels

| Feature | Set Name | Center frequency ± offset frequencies (bandwidths) [GHz] |
|---|---|---|
| water vapor | 183(3a) | 183.31 ± 1.5(1.4), 2.9(1.4), 4.5(1.8) |
| lines: | 183(3b) | 183.31 ± 1.5(1.4), 3.5(2.0), 7.0(3.0) |
| | 325(3a) | 325.15 ± 1.5(1.6), 3.2(1.8), 5.9(3.0) |
| | 325(3b) | 325.15 ± 1.5(1.6), 3.5(2.4), 9.5(3.0) |
| | 380(4) | 380.20 ± 0.9(0.8), 2.3(2.0), 4.6(2.6), 9.5(3.0) |
| | 448(3a) | 448.00 ± 1.4(1.2), 3.0(2.0), 7.2(3.0) |
| | 448(3b) | 448.00 ± 0.9(0.8), 2.5(2.2), 6.6(3.0) |
| | 620(3) | 620.70 ± 0.9(0.8), 2.0(1.6), 7.5(3.0) |
| | 916(3) | 916.17 ± 0.9(0.8), 2.8(2.6), 9.5(3.0) |
| oxygen | 425(3) | 424.76 ± 0.8(0.4), 1.8(1.0), 7.2(3.0) |
| lines: | 487(3) | 487.25 ± 0.7(0.4), 1.2(0.6), 8.0(3.0) |
| | 834(3) | 834.15 ± 0.7(0.4), 1.2(0.6), 9.5(3.0) |
| windows: | 220 | 220.0 ± 2.5(3.0) |
| | 243 | 243.2 ± 2.5(3.0) |
| | 280 | 280.0 ± 3.0(3.0) |
| | 344 | 344.0 ± 3.0(3.0) |
| | 462 | 462.4 ± 2.6(2.6) |
| | 643 | 642.9 ± 6.7(2.8) |
| | 664 | 664.0 ± 4.2(3.0) |
| | 683 | 683.0 ± 5.0(3.0) |
| | 874 | 874.4 ± 6.0(3.0) |

for being close to the geometric mean of two absorption line frequencies (e.g. 243 between 183 and 325 GHz or 280 between 183 and 425 GHz).

The frequencies were chosen by an interactive procedure involving viewing graphs of clear sky brightness temperature spectra and weighting function profiles. The brightness temperature spectra were created at a resolution of 0.05 GHz from absorption profiles generated by LBLRTM (version 6.12) for mean tropical and midlatitude winter atmospheres. The particular bandpasses of the channels were chosen to avoid the numerous narrow ozone absorption lines. For channels centered on absorption lines the channel offset frequency and bandwidth were chosen using weighting function plots. These weighting functions are the vertical derivative of the transmission from 50 km ($d\mathcal{T}_\nu(50,z)/dz$) at a resolution of 0.5 km. The weighting functions are averaged over both sidebands assuming a rectangular bandpass. The bandwidths of the channels were chosen to be as wide as possible without overlapping adjacent channels and without unduly smearing out the weighting function. The frequency offsets from the receiver center frequency were chosen to spread the weighting function peaks out evenly in altitude with a spacing of 1.5 to 2.0 km between adjacent channels. For the 183, 325, and 448 GHz receivers, two sets of frequencies are selected with the first being the SWCIR set and the second having the weighting functions cover a wider altitude range. The maximum bandwidth used was 3.0 GHz.

Table 1 lists the 44 microwave frequencies considered in the study and provides the name that

Table 2: Wavelengths of 4 Infrared Channels

| Feature | Channel Name | Channel wavelength range [$\mu$m ] |
|---|---|---|
| water vapor band | 6.7 | 6.535-6.895 |
| window | 8.5 | 8.40-8.70 |
| window | 11.0 | 10.78-11.28 |
| window | 12.0 | 11.77-12.27 |

each set of frequencies for one receiver will be referred to later. Figures 1 to 5 show the weighting functions for both atmospheres for all 44 microwave channels. The infrared channels were chosen to match four of those on MODIS, as listed in Table 2.

## 3. Bayesian Retrieval Algorithm

The retrieval algorithm used in the simulations is a Bayesian integration method (Evans et al., 2002). This algorithm is computationally efficient, introduces *a priori* information in a clearly defined manner, and retrieves uncertainty estimates along with ice cloud parameters and water vapor profiles. The Bayesian retrieval algorithm is based on Bayes theorem of probability theory:

$$p_{post}(x|T) = \frac{p_f(T|x)p_p(x)}{p_p(T)}$$

where $x$ is the vector of cloud and atmosphere parameters, and $T$ is the vector of measured brightness temperatures or radiances. The prior probability density function (pdf) $p_p(x)$ represents our knowledge of the atmospheric column before taking a measurement. The conditional pdf $p_f(T|x)$ is the distribution of brightness temperatures given an atmospheric state, which is closely related to the forward radiative transfer problem. The forward pdf is assumed to be a normal distribution of measurement error around brightness temperatures simulated by a radiative transfer model, $T_{sim,j}$, i.e.

$$p_f(T|x) = \prod_{j=1}^{M} N[(T_{sim,j}(x) - T_{obs,j})/\sigma_j] \ ,$$

where $T_{obs,j}$ is the $j$'th brightness temperature with measurement/modeling error of $\sigma_j$. The resulting posterior pdf $p_{post}(x|T)$ gives the probability distribution of the atmospheric parameters given the measurement.

A retrieval is made by integrating the posterior pdf to find the mean parameter vector, $x_{ret}$. A Monte Carlo integration is performed over the high dimensional parameter space by randomly generating the atmospheric parameters for many cases. To have an efficient algorithm the simulated brightness temperatures for these cases are precomputed with a radiative transfer model and stored in a database. The random cases in the database are distributed according to the prior pdf. This simplifies the Bayes integral for the retrieved vector to

$$\mathbf{x}_{ret} = \frac{\sum_i \mathbf{x}_i \ \exp\left[-\frac{1}{2}\chi_i^2\right]}{\sum_i \exp\left[-\frac{1}{2}\chi_i^2\right]} \qquad \mathbf{x}_i \text{ from } p_p(\mathbf{x})$$

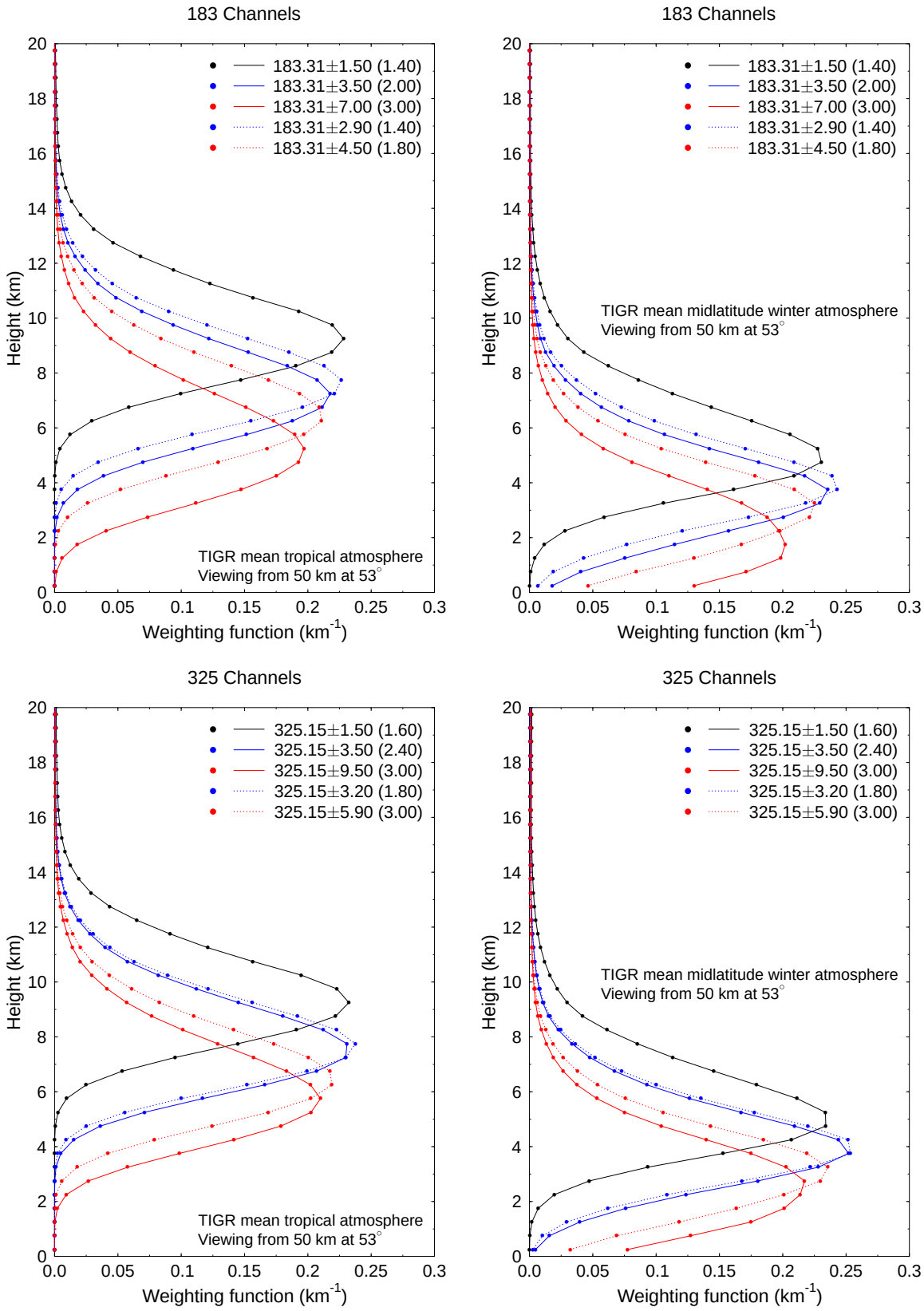


Figure 1: Weighting functions for 183 and 325 GHz channels.

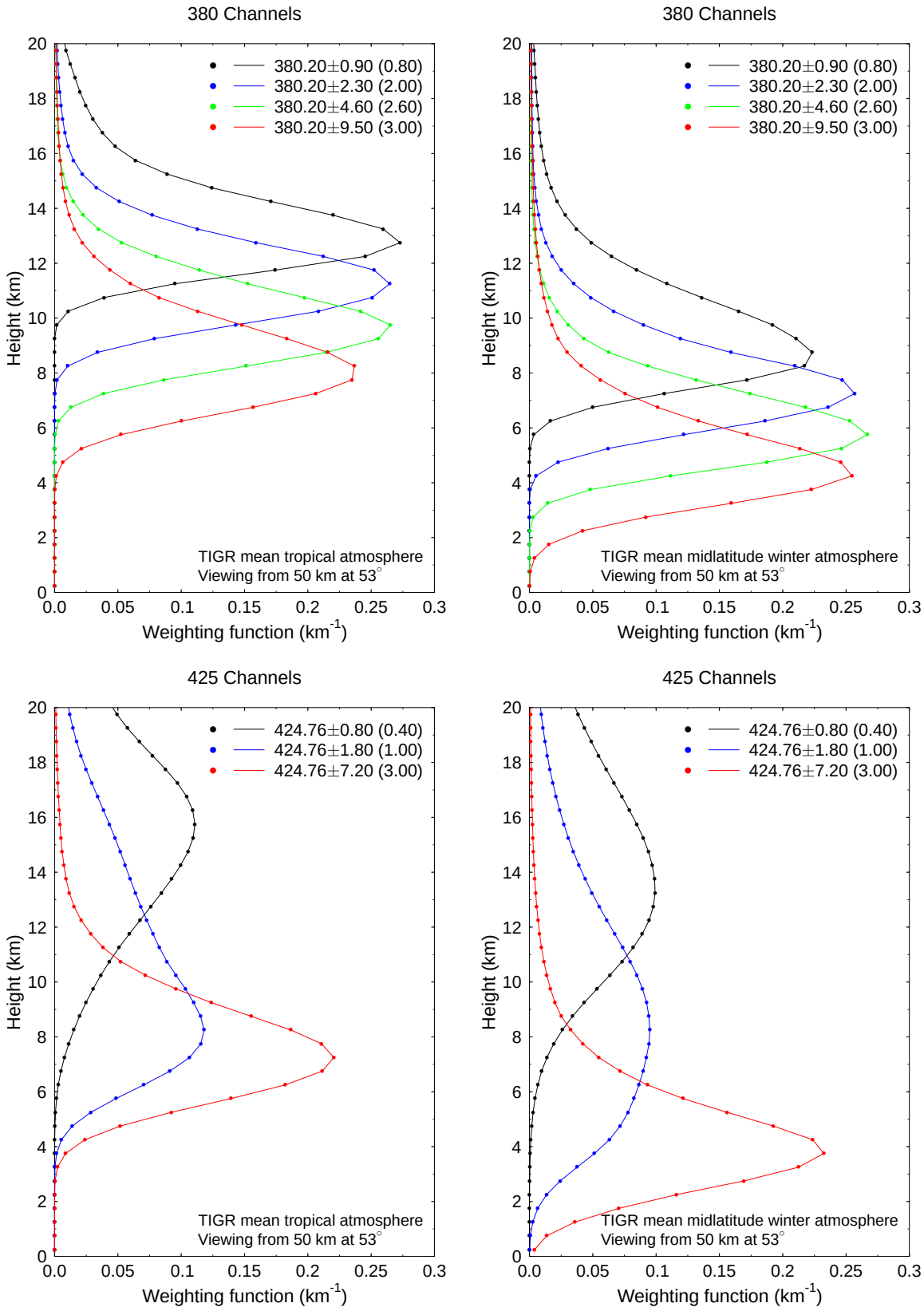


Figure 2: Weighting functions for 380 and 425 GHz channels.

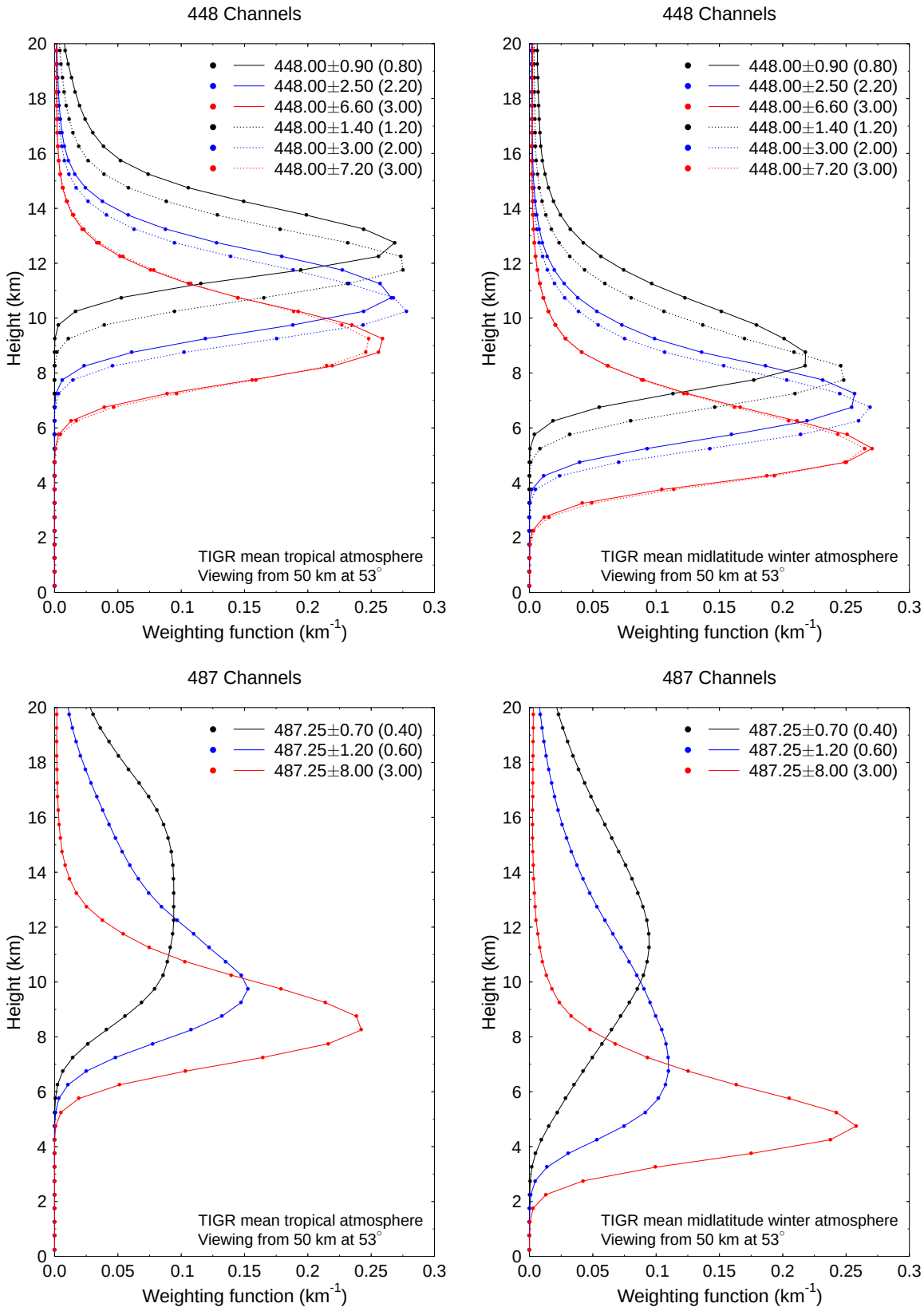


Figure 3: Weighting functions for 448 and 487 GHz channels.

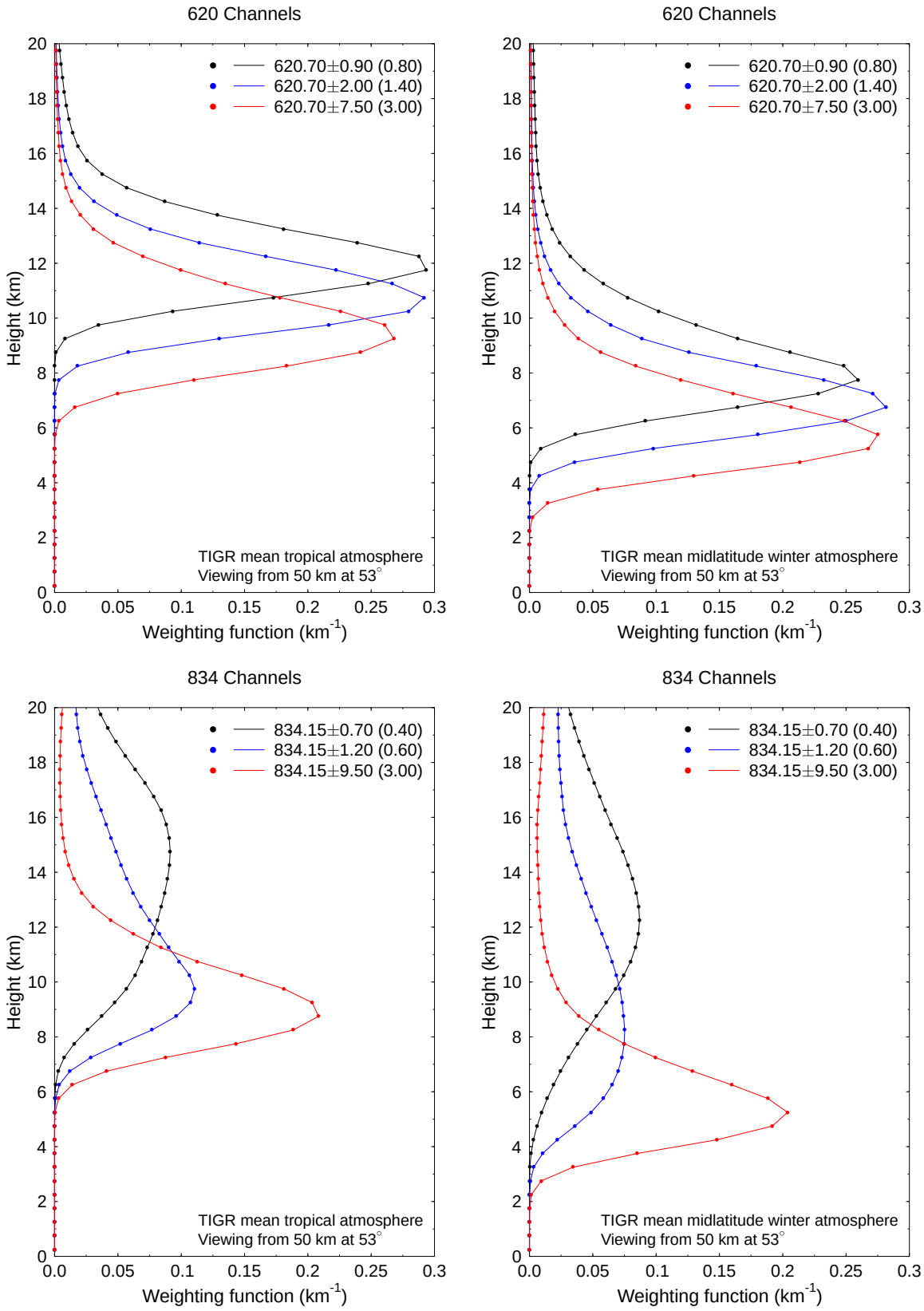


Figure 4: Weighting functions for 620 and 834 GHz channels.

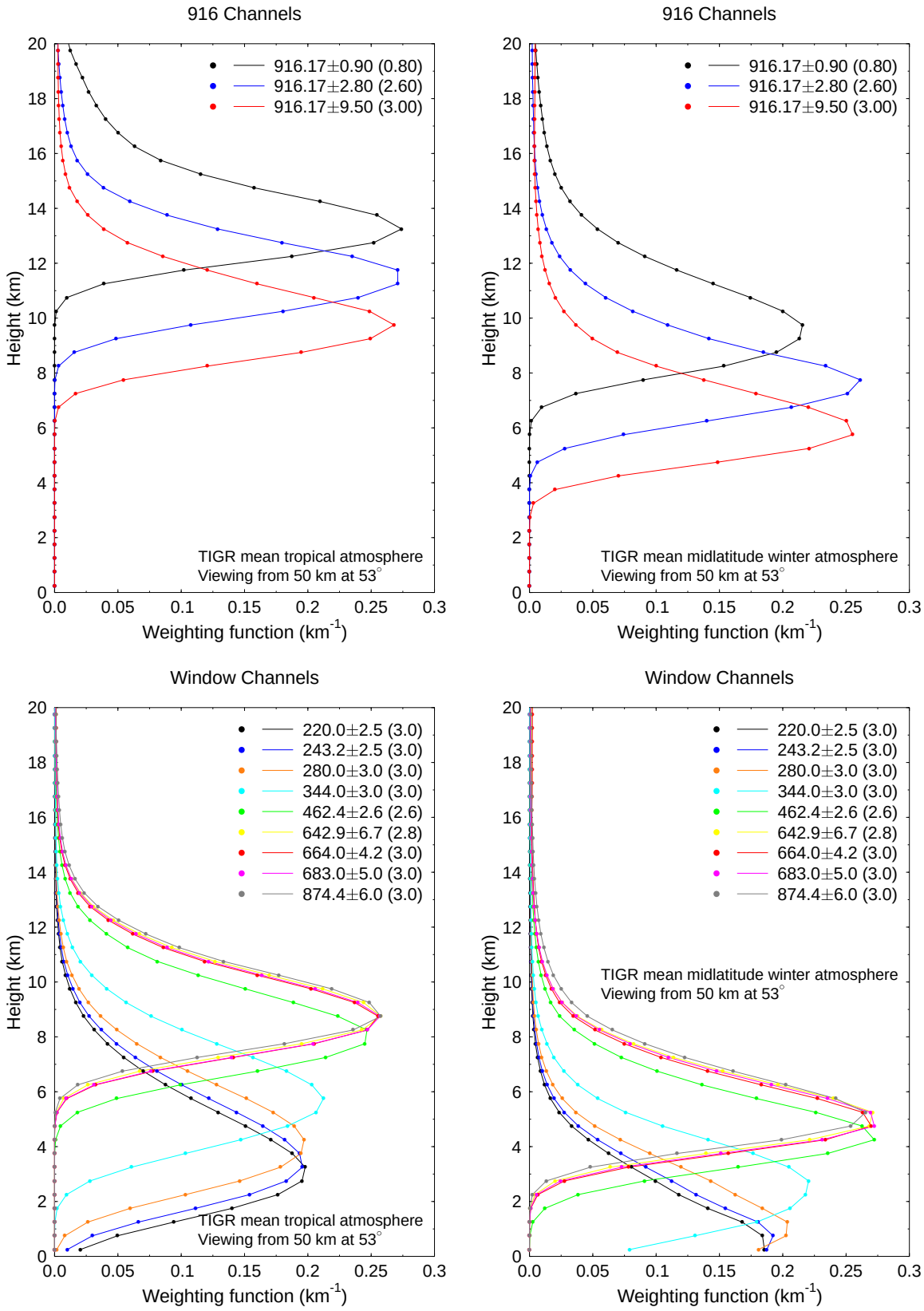


Figure 5: Weighting functions for 916 GHz and window channels.

where $\chi^2$ is the usual normalized measure of the disagreement between the observed and database brightness temperature vectors,

$$\chi_i^2 = \sum_{j=1}^{M} \frac{[T_{obs,j} - T_{sim,j}(\mathbf{x}_i)]^2}{\sigma_j^2} \quad .$$

A similar summation over database cases gives the standard deviation around the mean vector, which is an estimate of the uncertainty in the retrieval.

If the measurement noise is gaussian, as it is in the simulations described below, then the expected value of $\chi^2$ is $M$, where $M$ is the number of channels, and the standard deviation of $\chi^2$ is $\sqrt{M}$ for $M \gg 1$. The Bayesian integration algorithm requires a minimum number of database points (25 in the retrievals below) within a specified $\chi^2$ threshold, here set to $M + 4\sqrt{M}$. If there are fewer than the required number of points within this threshold due to the finite number of points in the database, then a larger $\chi^2$ range is considered by effectively increasing all the $\sigma_j$'s in steps of a factor of $\sqrt{2}$ until the minimum number of points is reached. This implies that there is a source of retrieval error due to the finite database size. Since the points in the database are distributed according to the prior pdf, there are few cases with high IWP. The database generation procedure has the option of rejecting low IWP cases according to an exponential probability distribution in IWP and increasing the weight of the remaining cases so that the high IWP enriched retrieval database is statistically equivalent to the prior pdf. This procedure improves the problem of not having enough database points within the required $\chi^2$ threshold for higher IWP.

## 4. Retrieval Database Generation

Generation of the database of atmospheric parameters and corresponding brightness temperatures is the key element of the Bayesian algorithm. The first step in generating the database is to create random profiles of temperature, water vapor, liquid and ice cloud properties such as water content and median particle size, and surface emissivity. The distribution of these parameters is the a priori information in the retrieval, so it is important that the profiles are realistic and completely cover the possible parameter range. The parameters that specify the cloudy atmospheric profiles are chosen from joint probability distributions, instead of using observed profiles. This is necessary because up to one million profiles may be generated and the Monte Carlo integration requires that each case be independent. Since the atmosphere and cloud parameters in the database are distributed according to the prior pdf, there are separate databases for different seasons and regions of the globe.

The second part of generating the database is to simulate the submillimeter and infrared observations with a radiative transfer model. A fast Eddington second approximation method is used. The microwave and infrared radiances are simulated for a viewing zenith angle of 53.1° (cosine is $\mu = 0.6$). The microwave radiances are converted to brightness temperature after the radiative transfer calculation (which is important since submillimeter frequencies are not in the Rayleigh-Jeans limit). For efficiency the monochromatic absorption profiles for an input atmosphere are interpolated in temperature and water vapor from reference profiles calculated with LBLRTM. Double sideband brightness temperatures are calculated with two monochromatic radiative transfer computations (which is a good approximation for the narrow bandwidths used here). Infrared channel radiances are computed with a pseudo-k-distribution approach that performs a weighted

sum of 4 to 6 strategically placed monochromatic calculations across the spectral band. The single scattering information for gamma particle size distributions is calculated for randomly oriented nonspherical particles with the Discrete Dipole Approximation (DDA) for the microwave channels and using volume and area equivalent sphere Mie scattering for infrared channels. A much slower multistream radiative transfer method is available to simulate polarization of the brightness temperature signal from horizontally or randomly oriented particles (see section 7.).

The retrieval database temperature and relative humidity profiles are generated with the correct statistics and vertical correlations using principal component analysis. The principle components are calculated from 118 tropical or 72 midlatitude winter TIGR3 profiles. A random profile is generated by setting the principle component coefficients to an independent normally distributed random deviate with the appropriate variance. The mean and variability of the temperature and relative humidity profiles from 10,000 realizations is shown in Fig. 6.

Multilayer ice clouds, mixed phase clouds, midlevel and boundary layer water clouds are generated with realistic geometric properties. There may be one or two ice cloud layers. Part of an "ice cloud" may be mixed phase or even liquid with a probability that depends on temperature. The choice of the cloud geometry distributions is loosely based on observed cloud height and thickness distributions obtained from radar. The upper ice cloud top height is gaussian distributed, the gap distance between the two ice clouds and all cloud thicknesses are exponentially distributed. All of the distributions are independent.

The microphysical properties of the ice clouds in the databases are based on in situ 2D-C probe observations of cirrus. The midlatitude winter simulation uses 3477 cirrus size distributions from the Atmospheric Radiation Measurement Cloud Intensive Operation Period (IOP) in March 2000 (Heymsfield et al., 2002). The 2D-C/2D-P probe number concentration as a function of maximum particle diameter for flights on March 5, 9, and 12 is converted to moments of equivalent sphere diameter using the effective density - diameter fitted relation presented in Fig. 15 of Heymsfield et al. (2002). This density - diameter relation gave better agreement between the 2D probe derived ice water content (IWC) and the IWC measured by the counterflow virtual impactor (CVI) than did the density-area ratio relation presented in the paper. The IWC and $D_{me}$ of a gamma distribution (with $\alpha = 1$) are obtained from the third and the fourth equivalent sphere diameter moments for each 5 second size distribution sample. The tropical simulation uses 3000 size distributions from the CEPEX experiment in 1993 (McFarquhar and Heymsfield, 1996) as described in Evans et al. (2002).

The cirrus microphysical generation procedure uses the observed relationship between IWC, $D_{me}$, and temperature. The parameters of a trivariate normal distribution are specified with the 3x3 covariance matrix of $\ln$(IWC), $\ln(D_{me})$, and temperature derived from the observed size distributions. Table 3 lists the the microphysical statistics that are input to the cloud generation procedure for the two simulations. The randomly generated ice cloud heights and thicknesses are used to index into the random temperature profiles to get cloud top and bottom temperatures. Given the top and bottom temperature, the IWC and $D_{me}$ at the top and bottom of the cloud are generated randomly from the log-normal distribution. The $D_{me}$ varies linearly with height inside the cloud, while the IWC varies as a power law in $D_{me}$. The bottom IWC and $D_{me}$ are required to be larger than cloud top values. This procedure simulates the observed cirrus microphysical relationships, such as smaller particles at colder temperatures and lower IWC with smaller particles.

Ice particle shape is effectively an error source in the ice cloud retrievals. Since the shapes of ice crystals in particular cloud types is relatively unknown and highly variable, the approach taken

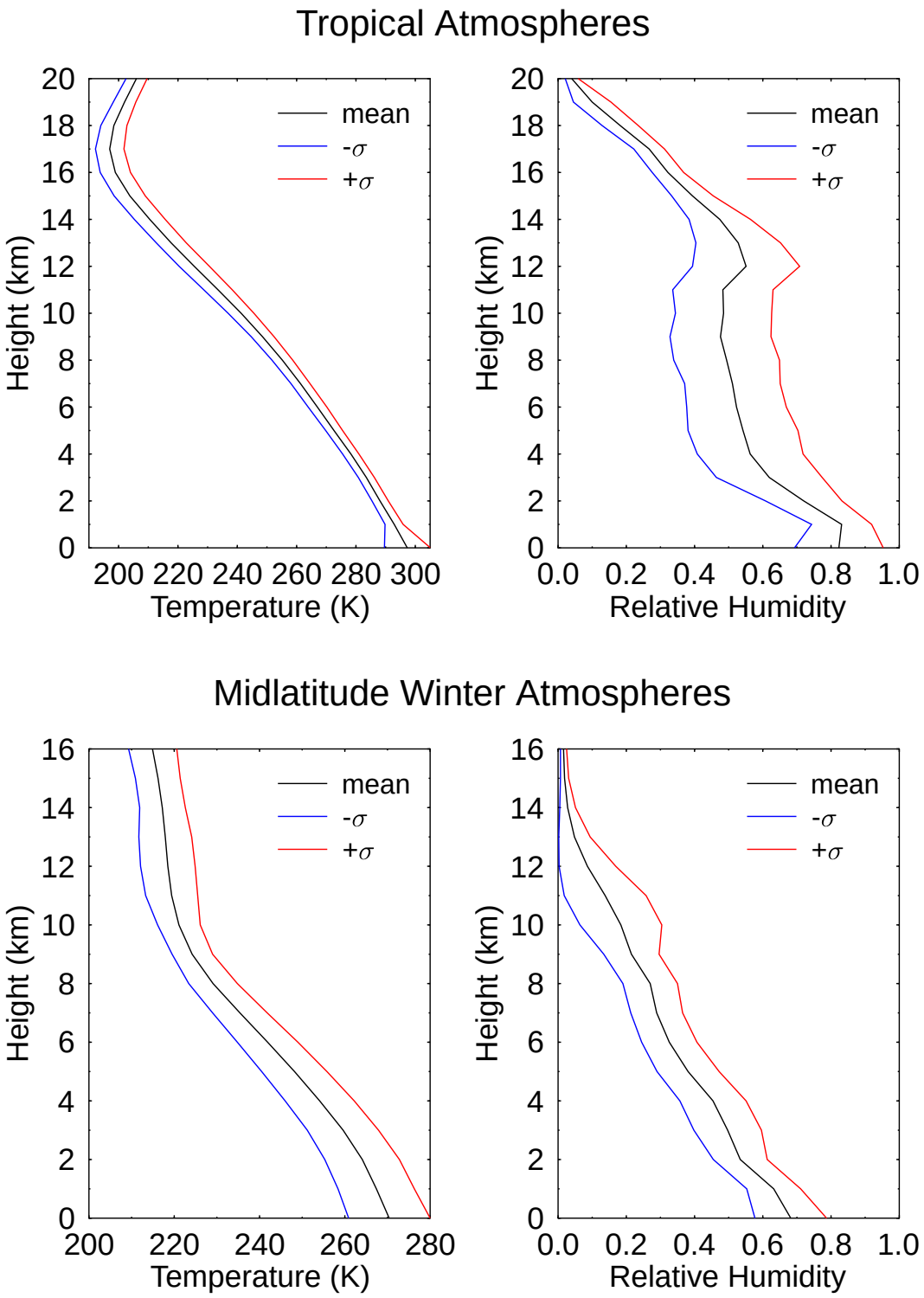


Figure 6: The mean and mean $\pm$ one standard deviation profiles of temperature and relative humidity from 10,000 randomly generated profiles for the tropical and midlatitude winter simulations.

Table 3: Microphysical Input Statistics

| | Temperature (K) | $\ln(\mathrm{IWC}[\mathrm{g/m^2}])$ | $\ln(D_{me}[\mu\mathrm{m}])$ |
|---|---|---|---|
| | ARM2000 Midlatitude Winter | | |
| mean | 241.5 | -4.01 | 5.37 |
| std. dev. | 12.9 | 1.59 | 0.63 |
| correlation | $\rho_{T-IWC}$ =0.534 | $\rho_{T-D_{me}}$ =0.728 | $\rho_{IWC-D_{me}}$ =0.745 |
| | CEPEX Tropical Anvils | | |
| mean | 230.3 | -4.53 | 4.95 |
| std. dev. | 11.8 | 2.07 | 0.59 |
| correlation | $\rho_{T-IWC}$ =0.322 | $\rho_{T-D_{me}}$ =0.618 | $\rho_{IWC-D_{me}}$ =0.733 |

here is to bracket the range of particle shapes in terms of their radiative properties. In the randomly oriented particle framework, the primary consideration is the particle bulk density or, equivalently, the ratio of surface area to mass. At both microwave and infrared wavelengths highly compact particles have considerably different scattering properties than more spread out particles. The two particle shapes used for the retrieval database are solid ice spheres (most compact) and 7-bullet rosettes (least compact). A single particle shape is randomly chosen for each cloud. The width of the ice particle gamma distribution is also randomly chosen for each cloud ($\alpha$ =0, 1, or 2 in the distribution defined by $N(D_e) \propto D_e^{\alpha} \exp[-(\alpha+3.67)D_e/D_{me}]$, where $D_e$ is the equivalent sphere diameter). The solid spheres have $D_{me}$ between 20 and 1000 $\mu$m , while the bullet-rosettes have $D_{me}$ between 25 and 400 $\mu$m (limited by the DDA technique and microphysical considerations).

The mixed phase procedure first decides whether the cloud is a pure water or ice cloud. The probability of a cloud being a pure water cloud depends linearly on the cloud top temperature between two specified temperature values (and is 0 below and 1 above the range). The probability of a cloud being a pure ice cloud depends linearly on the cloud base temperature. If a cloud is not a pure water cloud, and is not a pure ice cloud, then it is mixed phase. The mass fraction of water depend linearly on height within the cloud according to random water fractions chosen for the cloud top and base. The water fraction at cloud top and base is a triangular distribution with halfwidth of 0.25, and the mean varies linearly in height with a value of 0 at the level of homogeneous freezing (-39°C) and a value of 1 at the melting level. The water fraction is set to 0 above the homogeneous freezing level and 1 below the melting level. The total water content at cloud top and base is derived from the ice microphysics statistics. The liquid droplet median mass diameter is normally distributed (uniform within a cloud) with a mean of 18 $\mu$m and standard deviation of 4 $\mu$m . There may also be a specified probability of having a boundary layer water cloud. The boundary layer cloud has an exponential distribution of cloud top height (which is really an effective cloud height, since the cloud fraction is unity). The liquid water content of the boundary layer cloud is 0.3 g/m$^3$, and the median mass droplet diameter is normally distributed as for the other liquid clouds.

The surface has a small contribution for the lower altitude sensing channels from 183 to 344 GHz in drier atmospheres. A normally distributed surface emissivity with a mean of 0.93 and standard deviation of 0.03 is assumed. The surface emissivity is independent for four separate

Table 4: Parameters of the probability distributions describing the cloud geometry and phase

| Parameter | Tropical | | Midlat. Winter | |
|---|---|---|---|---|
| | Retrieval | Testing | Retrieval | Testing |
| Probability of two ice cloud layers | 0.0 | 0.33 | 0.0 | 0.33 |
| Temperature of mean cloud top height (K) | 225 | 210 | 238 | 226 |
| Standard deviation of cloud top height (km) | 2.5 | 2.0 | 2.0 | 1.0 |
| Mean upper cloud thickness (km) | 2.5 | 1.0 | 2.0 | 1.0 |
| Mean cloud gap distance (km) | - | 1.0 | - | 1.0 |
| Mean lower cloud thickness (km) | - | 2.0 | - | 1.5 |
| Pure water cloud top temp. range (K) | | 248–268 | | |
| Pure ice cloud bottom temp. range (K) | | 238–273 | | |
| Probability of boundary layer cloud | 0.25 | 0.33 | 0.0 | 0.0 |
| Mean boundary layer cloud top height (km) | 0.5 | 0.5 | - | - |

frequency ranges (around 183 GHz, 220-280 GHz, around 325 GHz, and above 380 GHz). The infrared surface emissivity is normally distributed with a mean of 0.97 and standard deviation of 0.01, and is independent for each of the three surface sensing channels (8.5, 11, 12 $\mu$m ).

## 5. Retrieval Simulation Procedures

The synthetic SIRICE observations for the retrieval simulations are made with the same procedure as used to generate the retrieval database profiles. It is not realistic, however, to use the same statistics for the testing database as for the retrieval database because the cirrus cloud statistics are not well known. Therefore, the testing and retrieval databases have the following differences:

1. The testing database has one or two independent ice cloud layers with different statistics from the single layer ice clouds in the retrieval database. Table 4 gives the retrieval and testing database cloud geometry parameters for the two simulations.

2. The testing database cirrus microphysical statistics are altered from the retrieval database by multiplying the IWC values by 2, but keeping the other parameters of the trivariate ($\ln$(IWC), $\ln(D_{me})$, $T$) normal distribution fixed.

The two retrieval databases, one for the tropical simulation and one for the midlatitude winter simulation, are generated with 1,000,000 cases each. The upper tropospheric water vapor profile is retrieved in five 2 km thick layers from 16 to 6 km altitude in the tropical simulation and 12 to 2 km altitude in the midlatitude winter simulation. The retrieved quantity is the integrated water vapor density (g/m$^2$) in each layer.

The statistics of the 10,000 randomly generated clouds used for testing are listed in Table 5. There is a wide range in each of the cloud parameters. The typical cirrus cloud has a somewhat smaller $D_{me}$ in the tropical simulation than in the midlatitude winter simulation, but a larger IWP. There are mixed phase clouds in 6.7% of the tropical cases and 8.9% of the midlatitude winter

Table 5: Statistics of the randomly generated ice clouds used for testing[a]

| Tropical Simulation | | | | | |
|---|---|---|---|---|---|
| Parameter | mean | median | std. dev. | minimum | maximum |
| IWP (g/m$^2$) | 108 | 15.9 | 381 | 0.01 | 7925 |
| $D_{me}$ ($\mu$m) | 139 | 117 | 84 | 25 | 787 |
| $Z_{medIWP}$ (km) | 12.8 | 12.9 | 2.2 | 5.6 | 20.5 |
| $Z_{top}$ (km) | 13.9 | 13.9 | 1.9 | 7.5 | 20.7 |
| $Z_{bot}$ (km) | 12.3 | 12.4 | 2.4 | 3.8 | 20.4 |

| Midlatitude Winter Simulation | | | | | |
|---|---|---|---|---|---|
| Parameter | mean | median | std. dev. | minimum | maximum |
| IWP (g/m$^2$) | 31.2 | 9.7 | 71.0 | 0.02 | 1691 |
| $D_{me}$ ($\mu$m) | 182 | 165 | 81 | 28 | 773 |
| $Z_{medIWP}$ (km) | 7.8 | 7.6 | 2.0 | 0.0 | 16.7 |
| $Z_{top}$ (km) | 8.8 | 8.6 | 1.7 | 3.0 | 17.4 |
| $Z_{bot}$ (km) | 7.3 | 7.3 | 2.2 | 0.0 | 16.6 |

[a]IWP is ice water path, $D_{me}$ is median mass equivalent sphere diameter, $Z_{medIWP}$ is height of median ice water path, $Z_{top}$ is maximum cloud top height, and $Z_{bot}$ is lowest ice particle height.

cases. For the tropical simulation 18.6% of the clouds have $\mathrm{IWP} < 2\ \mathrm{g/m^2}$, while for the midlatitude winter simulation 19.6% have $\mathrm{IWP} < 2\ \mathrm{g/m^2}$. However, less than 0.6% of the total ice mass is contained in clouds with $\mathrm{IWP} < 2\ \mathrm{g/m^2}$ for both simulations. The distinction between the fraction of clouds and the fraction of total IWP is important, since the goal of the measurements is to sense total regional ice mass, not individual cloud IWP.

Along with the microwave and infrared channels, the temperature profile may be an observable. This is to simulate a retrieval algorithm using temperature profiles obtained from numerical weather prediction (NWP) models (which in turn obtain temperature from other satellite sensors). The temperature profile is specified as the average temperature of the same five 2 km thick layers used for the water vapor retrievals. Gaussian distributed noise with an rms of 1.5 K is added to each layer temperature observable, as this is approximately the level of accuracy achieved by present day NWP models.

Gaussian distributed noise with the appropriate amplitude is added to the microwave brightness temperatures simulated by the radiative transfer model. The noise rms for each channel is derived from an assumed system temperature ($T_{sys}$), integration time ($t_{int}$), and the bandwidth $B$ by

$$NE\Delta T = \frac{T_{sys}}{\sqrt{Bt_{int}}} \ .$$

Receiver technology indicates that higher frequencies have higher system temperatures, so the formula $T_{sys} = 900\ \mathrm{K} + (3\ \mathrm{K/GHz})f$, where $f$ is the frequency, is assumed based on the lowest noise receivers measured at JPL. The integration time is taken to be $t_{int} = 3$ ms. The absolute calibration and radiative transfer model error is assumed to be 1.0 K and is added in quadrature to

obtain the noise rms for each channel: $\sigma_j^2 = (1.0\ \mathrm{K})^2 + NE\Delta T_j^2$. The $\sigma$'s range from about 1.1 K for the 243 GHz channel to 1.5 K for the 874 GHz channel, with one of the narrower bandwidth high-frequency channels having $\sigma = 3.3$ K. The rms of the gaussian noise for the infrared channels is based on 0.5 K NE$\Delta T$ at 260 K scene temperature, resulting in $\sigma = 0.6$ mW cm/(m$^2$ st) for the 11 and 12 $\mu$m channels.

## 6. Channel Selection Retrieval Simulation Results

The number of possible combinations of the 44 microwave channels, 4 infrared channels, and 5 temperature layer observables is much too large to perform retrieval simulations for each one. Instead, particular channel sets are constructed based on principles known to be relevant for ice cloud sensing. These are that a wide range of microwave frequencies should be covered and the frequencies should be roughly equally spaced in a logarithmic sense. The 26 sets of microwave channels referenced A to Z are listed in Table 6. Most of the sets require six receivers (ignoring the issue of multiple receivers for orthogonal polarizations). Set A has the CIWSIR frequencies with 5 receivers. Set B adds the 243 GHz receiver and changes the 683 GHz receiver to 664 GHz. Sets C and D explore the difference between the SWCIR and wider sets of bandpasses on 183, 325, and 448 GHz receivers. Sets E to H look at the placement of the 220-280 GHz and 640-680 GHz window channel receivers. Sets I to L explore using absorption line channels instead of the 664 GHz and 874 GHz window channels, while set M tries using only window channels (except for 183 GHz channels). Sets N to P look at using different sets of absorption lines including the 487 and 425 GHz oxygen lines. Sets Q through Z explore options with less than six receivers. Set Q has five receivers, sets R to W have four receivers, and sets X to Z have three receivers.

Six sets of the four infrared channels are considered, referenced by numbers 1 to 6. These sets range from one channel to all four (see Table 6). The nomenclature for sets that combine microwave and infrared channels is to combine the microwave letter with the infrared number, as in "C3". The addition of the five layers of temperature profile information is indicated by an additional lowercase t, as in "Ct" or "C3t". Retrievals without microwave channels are indicated by "_", as in "_3" which uses only infrared channels.

Retrieval simulations were first performed for all the microwave channel sets. One of the best microwave sets (the "likely candidate") was then combined with each of the six infrared sets. Retrieval simulations were done for all 26 microwave sets in combination with one infrared set. Simulations were also done for the selected microwave and microwave+infrared set combined with the temperature profile information.

The ice cloud IWP, $D_{me}$, and $Z_{medIWP}$ retrieval errors are assessed by comparing the retrieved parameters to the known values. Since IWP varies by orders of magnitudes, the error is expressed in a fractional sense using the logarithmic difference expressed in decibels (dB) (i.e. $4.343 \ln(\mathrm{IWPret}/\mathrm{IWPtrue})$). The fractional error is usually applied to cases with IWP above 2 g/m$^2$ because a fractional error for IWP near zero is meaningless. $D_{me}$ errors are also expressed in dB, while $Z_{medIWP}$ errors are in km. Instead of the rms difference, a more robust statistic, the median of the absolute value of the error is used. Thus, over all the retrievals being combined for an error estimate, 50% have a dB error less than the median error, and 50% have a larger error. For a zero mean gaussian distribution the root mean square error is 1.48 times the median absolute error. A 1 dB error is a factor of $10^{\pm 0.1}$ or about 25%, while a 3 dB error is a factor of 2. The rms water vapor errors in g/m$^2$ for each layer are normalized by the mean layer water vapor amount to

Table 6: Channel Sets Investigated

| Microwave Channel Sets | |
|---|---|
| Set | Channel names |
| A | 183(3a), 325(3a), 448(3a), 683, 874 (CIWSIR) |
| B | 183(3a), 243, 325(3a), 448(3a), 664, 874 |
| C | 183(3b), 243, 325(3b), 448(3a), 664, 874 |
| D | 183(3b), 243, 325(3b), 448(3b), 664, 874 |
| E | 183(3b), 220, 325(3b), 448(3a), 664, 874 |
| F | 183(3b), 280, 325(3b), 448(3a), 664, 874 |
| G | 183(3b), 243, 325(3b), 448(3a), 643, 874 |
| H | 183(3b), 243, 325(3b), 448(3a), 683, 874 |
| I | 183(3b), 243, 325(3b), 448(3a), 620(3), 874 |
| J | 183(3b), 243, 325(3b), 448(3a), 664, 916(3) |
| K | 183(3b), 243, 325(3b), 448(3a), 620(3), 916(3) |
| L | 183(3b), 243, 325(3b), 448(3a), 643, 834(3) |
| M | 183(3b), 243, 344, 462, 643, 874 |
| N | 183(3b), 243, 380(4), 487(3), 664, 874 |
| O | 183(3b), 243, 380(4), 487(3), 620(3), 834(3) |
| P | 183(3b), 243, 325(3b), 425(3), 620(3), 874 |
| Q | 183(3b), 243, 325(3b), 448(3a), 664 |
| R | 183(3b), 325(3b), 448(3a), 664 |
| S | 183(3b), 325(3b), 448(3a), 874 |
| T | 183(3b), 243, 380(4), 643 |
| U | 183(3b), 280, 425(3), 643 |
| V | 183(3b), 280, 425(3), 620(3) |
| W | 220, 325(3b), 448(3a), 664 |
| X | 183(3b), 325(3a), 448(3a) |
| Y | 183(3b), 448(3a), 664 |
| Z | 183(3b), 448(3a), 874 |

| Infrared Channel Sets | |
|---|---|
| Set | Channel names |
| 1 | 11.0 |
| 2 | 11.0, 12.0 |
| 3 | 6.7, 11.0, 12.0 |
| 4 | 8.5, 11.0, 12.0 |
| 5 | 6.7, 8.5, 12.0 |
| 6 | 6.7, 8.5, 11.0, 12.0 |

derive the rms fractional error. The water vapor error is also compared to the "natural variability" of water vapor by taking the ratio of the rms error to the standard deviation of water vapor amount for each layer.

Overall summary results of the retrieval simulations for all the channel sets are given in Tables 7 and 8. In addition to the ice cloud property and water vapor retrieval errors, the fraction of the retrievals that could be done without expanding the $\chi^2$ threshold is listed. This fraction is a measure of the overall retrieval error due to the finite size of the retrieval database. As more channels are added to the set and the retrievals become more constrained, it becomes more difficult to get 25 database points within the original $\chi^2$ threshold. For example, the fraction of tropical retrievals within the original $\chi^2$ threshold for the C set is 0.903, for the C3 set is 0.762, and for the C3t set is 0.426. This problem with retrieval error due to the finite database size can result in the retrieval error actually increasing when more channels are added. There is also a certain amount of stochastic noise in the retrieval due to the random cases in the retrieval database and the testing databases. These facts should be kept in mind when interpreting the retrieval simulation results.

The retrieval simulations are designed to be realistic, but the large uncertainties in ice cloud property statistics implies significant uncertainties in the overall magnitude of the retrieval errors. Of course, the two situations simulated (tropical and midlatitude winter) are not representative of all ice clouds. If the true statistics of ice clouds have higher IWP, larger particle sizes, or a smaller range of particle density, then the retrieval errors would decrease. Nevertheless, the general characteristics of the simulation results should be correct, such as the relative merits of particular channel sets. Because the statistics of ice cloud properties are unknown, it is important not to rely solely on the summary numbers listed in the tables, but also to compare the channel set retrieval errors as a function of IWP, $D_{me}$, and cloud height.

Scanning the summary results listed in the tables, it appears that the best microwave channel set is I and the best infrared channel set is 5, though there are several sets that have about the same retrieval accuracy. However, here microwave set C and infrared set 3 are singled out for closer investigation. The overall characteristics of the ice cloud retrieval errors, and how the errors change with the addition of infrared and temperature information, can be seen in graphs of the IWP, $D_{me}$, and $Z_{medIWP}$ errors in Figs. 7 to 10. The addition of temperature information to the microwave channels (Ct vs. C) does not improve the IWP and $D_{me}$ retrievals, and indeed can make them worse due to the finite retrieval database error. The addition of the infrared channels improves the IWP retrievals very substantially, until the ice water path is so high that the IR is always saturated. The infrared channels dramatically improve the $D_{me}$ retrievals for small particles in the tropical simulation (Fig. 9), both because the IR has improved sensitivity to thin clouds and because the IR particle size sensitivity is limited to $D_{me}$ less than 100 $\mu$m . The IR channels do not improve the $D_{me}$ retrievals for small particles in the midlatitude winter simulation. As might be expected, the temperature information improves the retrievals of the median IWP height ($Z_{medIWP}$) as do the infrared channels for smaller IWP in the tropical simulation (Fig. 10). With temperature profile information the median error in $Z_{medIWP}$ is less than about 0.3 km for IWP$>$50 g/m$^2$. It is worth noting that the ice cloud retrieval accuracy with three infrared channels alone is very poor compared to the microwave only or the microwave+infrared retrievals (see _3 entry in Table 8).

The comparison of the microwave channel sets can be done by grouping related sets together. Are the ice cloud retrievals improved by using the wider spaced channels on the 183, 325, and 448 GHz water vapor absorption lines? Fig. 11 shows sets B, C, and D, which compare the narrower and wider spaced channels. The figure and Table 7 indicate that the C set has slightly better

Table 7: Summary Results for Microwave only Channel Sets*

| | Tropical Simulation | | | | | Midlatitude Winter Simulation | | | | |
|---|---|---|---|---|---|---|---|---|---|---|
| | Median error | | | Vapor | Ret | Median error | | | Vapor | Ret |
| Set | IWP | $D_{me}$ | $Z_{med}$ | Error | Frac | IWP | $D_{me}$ | $Z_{med}$ | Error | Frac |
| A | 0.963 | 0.624 | 0.780 | 0.903 | 0.925 | 1.540 | 0.651 | 0.670 | 0.859 | 0.987 |
| B | 0.934 | 0.608 | 0.760 | 0.893 | 0.908 | 1.488 | 0.655 | 0.660 | 0.824 | 0.973 |
| C | 0.936 | 0.608 | 0.760 | 0.893 | 0.903 | 1.413 | 0.661 | 0.660 | 0.805 | 0.966 |
| Ct | 0.966 | 0.618 | 0.550 | 0.435 | 0.792 | 1.373 | 0.657 | 0.490 | 0.477 | 0.759 |
| D | 0.949 | 0.624 | 0.750 | 0.898 | 0.911 | 1.466 | 0.667 | 0.660 | 0.797 | 0.964 |
| E | 0.937 | 0.603 | 0.760 | 0.894 | 0.902 | 1.407 | 0.658 | 0.660 | 0.801 | 0.963 |
| F | 0.937 | 0.611 | 0.760 | 0.893 | 0.905 | 1.391 | 0.662 | 0.660 | 0.814 | 0.971 |
| G | 0.944 | 0.609 | 0.760 | 0.894 | 0.903 | 1.425 | 0.654 | 0.670 | 0.804 | 0.966 |
| H | 0.934 | 0.610 | 0.760 | 0.892 | 0.903 | 1.411 | 0.653 | 0.660 | 0.804 | 0.967 |
| I | 0.909 | 0.601 | 0.690 | 0.893 | 0.892 | 1.344 | 0.652 | 0.640 | 0.798 | 0.962 |
| J | 0.960 | 0.572 | 0.600 | 0.888 | 0.874 | 1.471 | 0.659 | 0.630 | 0.789 | 0.955 |
| K | 0.985 | 0.580 | 0.600 | 0.890 | 0.875 | 1.553 | 0.672 | 0.630 | 0.785 | 0.958 |
| L | 1.002 | 0.616 | 0.720 | 0.833 | 0.903 | 1.509 | 0.663 | 0.670 | 0.787 | 0.960 |
| M | 1.076 | 0.654 | 0.820 | 0.917 | 0.940 | 1.558 | 0.677 | 0.690 | 0.818 | 0.981 |
| N | 0.982 | 0.623 | 0.740 | 0.796 | 0.908 | 1.839 | 0.700 | 0.700 | 0.826 | 0.963 |
| O | 0.990 | 0.616 | 0.610 | 0.783 | 0.895 | 1.768 | 0.713 | 0.660 | 0.817 | 0.958 |
| P | 0.930 | 0.606 | 0.600 | 0.729 | 0.879 | 1.377 | 0.649 | 0.610 | 0.761 | 0.944 |
| Q | 1.147 | 0.686 | 0.780 | 0.891 | 0.918 | 1.558 | 0.690 | 0.680 | 0.806 | 0.974 |
| R | 1.158 | 0.696 | 0.790 | 0.891 | 0.926 | 1.562 | 0.693 | 0.690 | 0.822 | 0.984 |
| S | 0.952 | 0.631 | 0.770 | 0.894 | 0.920 | 1.425 | 0.662 | 0.670 | 0.820 | 0.982 |
| T | 1.195 | 0.750 | 0.810 | 0.880 | 0.935 | 2.075 | 0.786 | 0.740 | 0.839 | 0.982 |
| U | 1.315 | 0.804 | 0.810 | 0.722 | 0.946 | 1.905 | 0.750 | 0.740 | 0.791 | 0.982 |
| V | 1.330 | 0.760 | 0.620 | 0.724 | 0.920 | 1.870 | 0.749 | 0.650 | 0.782 | 0.975 |
| W | 1.150 | 0.752 | 0.810 | 0.897 | 0.936 | 1.568 | 0.740 | 0.710 | 0.824 | 0.984 |
| X | 1.582 | 0.800 | 0.820 | 0.890 | 0.945 | 1.976 | 0.746 | 0.740 | 0.821 | 0.990 |
| Y | 1.198 | 0.808 | 0.860 | 0.898 | 0.955 | 2.315 | 0.846 | 0.780 | 0.891 | 0.994 |
| Z | 1.055 | 0.711 | 0.830 | 0.901 | 0.950 | 2.226 | 0.817 | 0.760 | 0.890 | 0.993 |

*Median absolute error of ice water path (IWP), median mass equivalent sphere diameter ($D_{me}$), and height of median ice water path ($Z_{med}$) for cases with IWP above 2 g/m$^2$. "Vapor Error" is the average over the five layers of the ratio of rms error in layer water vapor amount (g/m$^2$) to the standard deviation of water vapor amount. "Ret Frac" is the fraction of the 10,000 retrievals that could be done without expanding the $\chi^2$ threshold.

Table 8: Summary Results for Sets Including Infrared Channels

| | Tropical Simulation | | | | | Midlatitude Winter Simulation | | | | |
|---|---|---|---|---|---|---|---|---|---|---|
| | Median error | | | Vapor | Ret | Median error | | | Vapor | Ret |
| Set | IWP | $D_{me}$ | $Z_{med}$ | Error | Frac | IWP | $D_{me}$ | $Z_{med}$ | Error | Frac |
| C1 | 0.549 | 0.449 | 0.720 | 0.913 | 0.812 | 0.839 | 0.588 | 0.680 | 0.789 | 0.871 |
| C2 | 0.536 | 0.449 | 0.710 | 0.927 | 0.777 | 0.851 | 0.591 | 0.690 | 0.797 | 0.825 |
| C3 | 0.510 | 0.425 | 0.660 | 0.920 | 0.762 | 0.844 | 0.583 | 0.690 | 0.799 | 0.812 |
| C4 | 0.510 | 0.444 | 0.690 | 0.931 | 0.723 | 0.840 | 0.598 | 0.680 | 0.794 | 0.794 |
| C5 | 0.496 | 0.422 | 0.660 | 0.919 | 0.724 | 0.834 | 0.593 | 0.670 | 0.792 | 0.814 |
| C6 | 0.494 | 0.422 | 0.660 | 0.925 | 0.705 | 0.839 | 0.587 | 0.680 | 0.793 | 0.782 |
| C3t | 0.555 | 0.460 | 0.510 | 0.474 | 0.426 | 0.887 | 0.589 | 0.520 | 0.514 | 0.303 |
| _3 | 2.389 | 1.320 | 1.200 | 0.985 | 0.997 | 3.741 | 1.157 | 1.310 | 0.975 | 0.997 |
| _3t | 2.436 | 1.335 | 1.090 | 0.661 | 0.956 | 3.533 | 1.165 | 1.150 | 0.589 | 0.901 |
| A3 | 0.515 | 0.437 | 0.670 | 0.920 | 0.804 | 1.080 | 0.602 | 0.680 | 0.845 | 0.907 |
| B3 | 0.511 | 0.432 | 0.670 | 0.916 | 0.771 | 0.919 | 0.595 | 0.680 | 0.813 | 0.838 |
| C3 | 0.510 | 0.425 | 0.660 | 0.920 | 0.762 | 0.844 | 0.583 | 0.690 | 0.799 | 0.812 |
| D3 | 0.507 | 0.430 | 0.660 | 0.917 | 0.771 | 0.880 | 0.591 | 0.680 | 0.790 | 0.791 |
| E3 | 0.504 | 0.430 | 0.670 | 0.922 | 0.759 | 0.854 | 0.588 | 0.690 | 0.795 | 0.793 |
| F3 | 0.504 | 0.424 | 0.670 | 0.919 | 0.764 | 0.867 | 0.583 | 0.680 | 0.804 | 0.839 |
| G3 | 0.513 | 0.422 | 0.670 | 0.918 | 0.765 | 0.858 | 0.587 | 0.690 | 0.799 | 0.811 |
| H3 | 0.505 | 0.417 | 0.670 | 0.920 | 0.763 | 0.844 | 0.590 | 0.700 | 0.797 | 0.812 |
| I3 | 0.488 | 0.426 | 0.640 | 0.921 | 0.742 | 0.835 | 0.588 | 0.670 | 0.793 | 0.802 |
| J3 | 0.474 | 0.421 | 0.580 | 0.921 | 0.707 | 0.829 | 0.590 | 0.660 | 0.787 | 0.774 |
| K3 | 0.498 | 0.429 | 0.580 | 0.926 | 0.714 | 0.892 | 0.606 | 0.650 | 0.790 | 0.782 |
| L3 | 0.532 | 0.443 | 0.640 | 0.868 | 0.758 | 0.876 | 0.590 | 0.700 | 0.789 | 0.782 |
| M3 | 0.563 | 0.448 | 0.690 | 0.921 | 0.814 | 0.879 | 0.594 | 0.690 | 0.804 | 0.858 |
| N3 | 0.534 | 0.431 | 0.630 | 0.833 | 0.745 | 1.100 | 0.656 | 0.710 | 0.800 | 0.786 |
| O3 | 0.533 | 0.460 | 0.580 | 0.821 | 0.728 | 1.044 | 0.659 | 0.680 | 0.803 | 0.766 |
| P3 | 0.488 | 0.422 | 0.560 | 0.766 | 0.680 | 0.841 | 0.592 | 0.630 | 0.760 | 0.712 |
| Q3 | 0.569 | 0.471 | 0.670 | 0.910 | 0.795 | 0.883 | 0.608 | 0.710 | 0.798 | 0.842 |
| R3 | 0.569 | 0.476 | 0.670 | 0.908 | 0.816 | 0.943 | 0.610 | 0.710 | 0.809 | 0.895 |
| S3 | 0.523 | 0.444 | 0.670 | 0.910 | 0.797 | 0.920 | 0.592 | 0.690 | 0.807 | 0.884 |
| T3 | 0.628 | 0.503 | 0.690 | 0.897 | 0.823 | 1.186 | 0.708 | 0.760 | 0.810 | 0.872 |
| U3 | 0.646 | 0.515 | 0.640 | 0.743 | 0.807 | 1.053 | 0.656 | 0.720 | 0.781 | 0.857 |
| V3 | 0.607 | 0.521 | 0.570 | 0.753 | 0.762 | 1.001 | 0.640 | 0.670 | 0.777 | 0.827 |
| W3 | 0.575 | 0.515 | 0.680 | 0.911 | 0.832 | 0.951 | 0.642 | 0.730 | 0.811 | 0.882 |
| X3 | 0.742 | 0.554 | 0.680 | 0.901 | 0.854 | 1.063 | 0.644 | 0.740 | 0.809 | 0.922 |
| Y3 | 0.618 | 0.540 | 0.710 | 0.907 | 0.863 | 1.502 | 0.764 | 0.780 | 0.852 | 0.940 |
| Z3 | 0.584 | 0.495 | 0.690 | 0.906 | 0.844 | 1.494 | 0.745 | 0.750 | 0.847 | 0.932 |

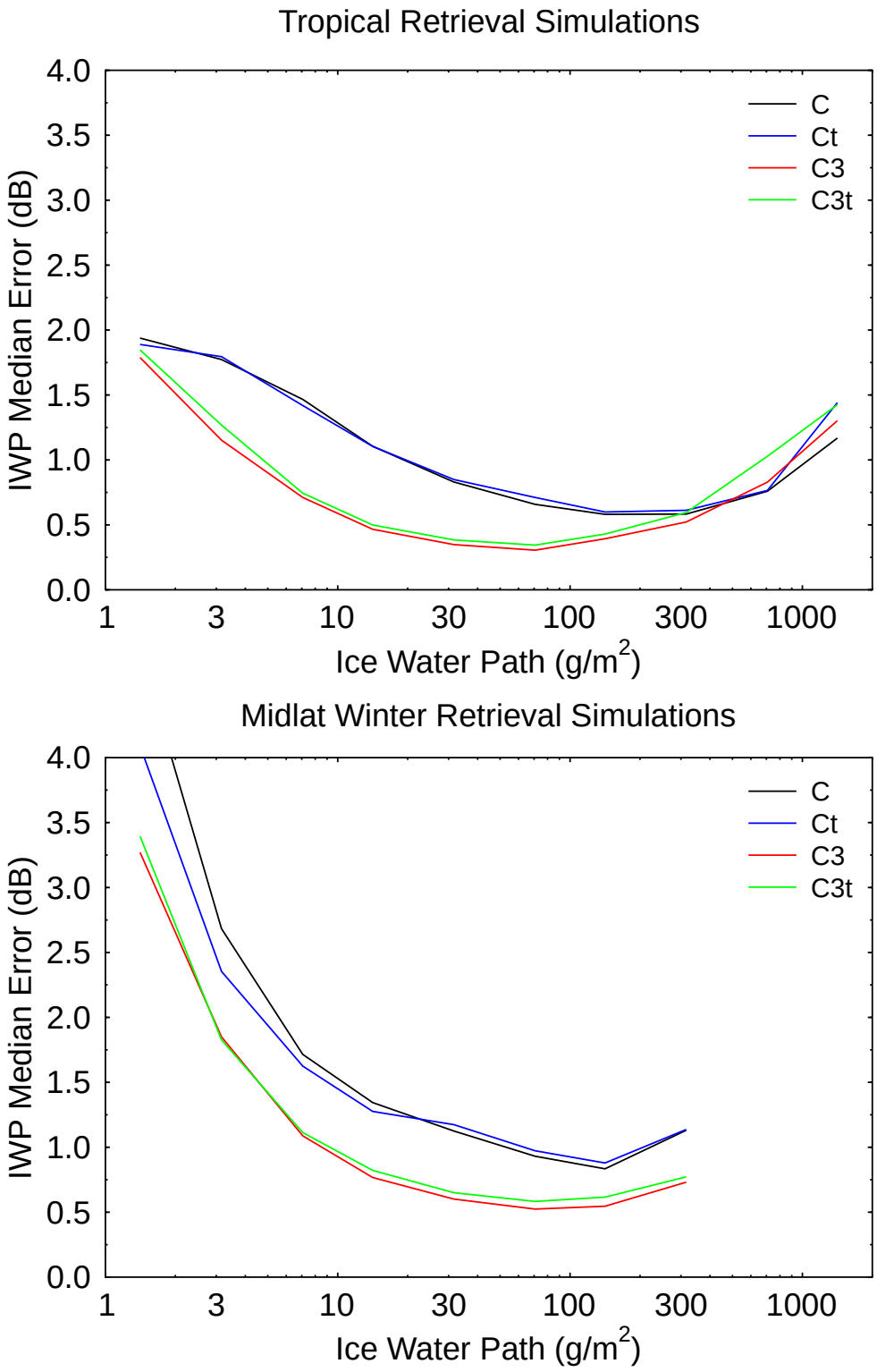
Tropical Retrieval Simulations
IWP Median Error (dB)
4.0
3.5
3.0
2.5
2.0
1.5
1.0
0.5
0.0
1
3
10
30
100
300
1000
Ice Water Path (g/m2)
C
Ct
C3
C3t
Midlat Winter Retrieval Simulations
IWP Median Error (dB)
4.0
3.5
3.0
2.5
2.0
1.5
1.0
0.5
0.0
1
3
10
30
100
300
1000
Ice Water Path (g/m2)
C
Ct
C3
C3t

Figure 7:

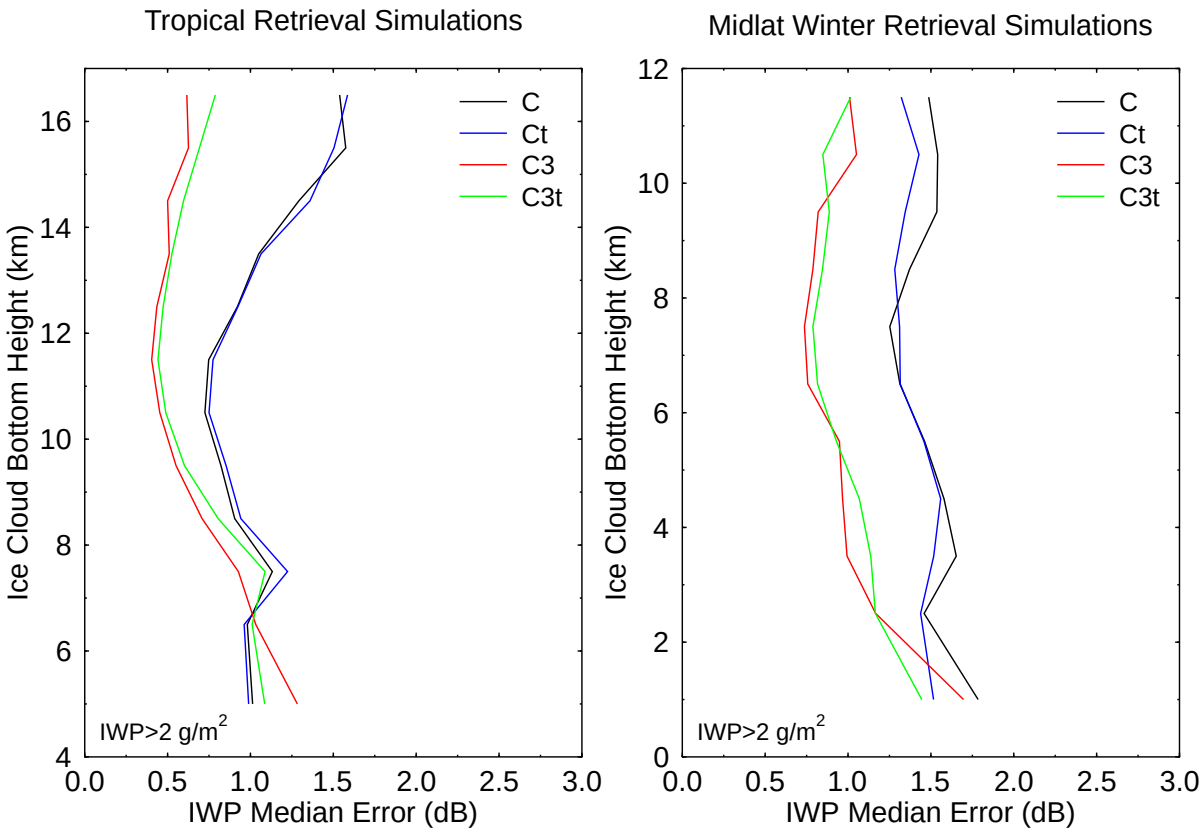
Tropical Retrieval Simulations
Midlat Winter Retrieval Simulations
Ice Cloud Bottom Height (km)
IWP Median Error (dB)
IWP>2 g/m2
C
Ct
C3
C3t
0.0
0.5
1.0
1.5
2.0
2.5
3.0
4
6
8
10
12
14
16
0
2
4
6
8
10
12

Figure 8:

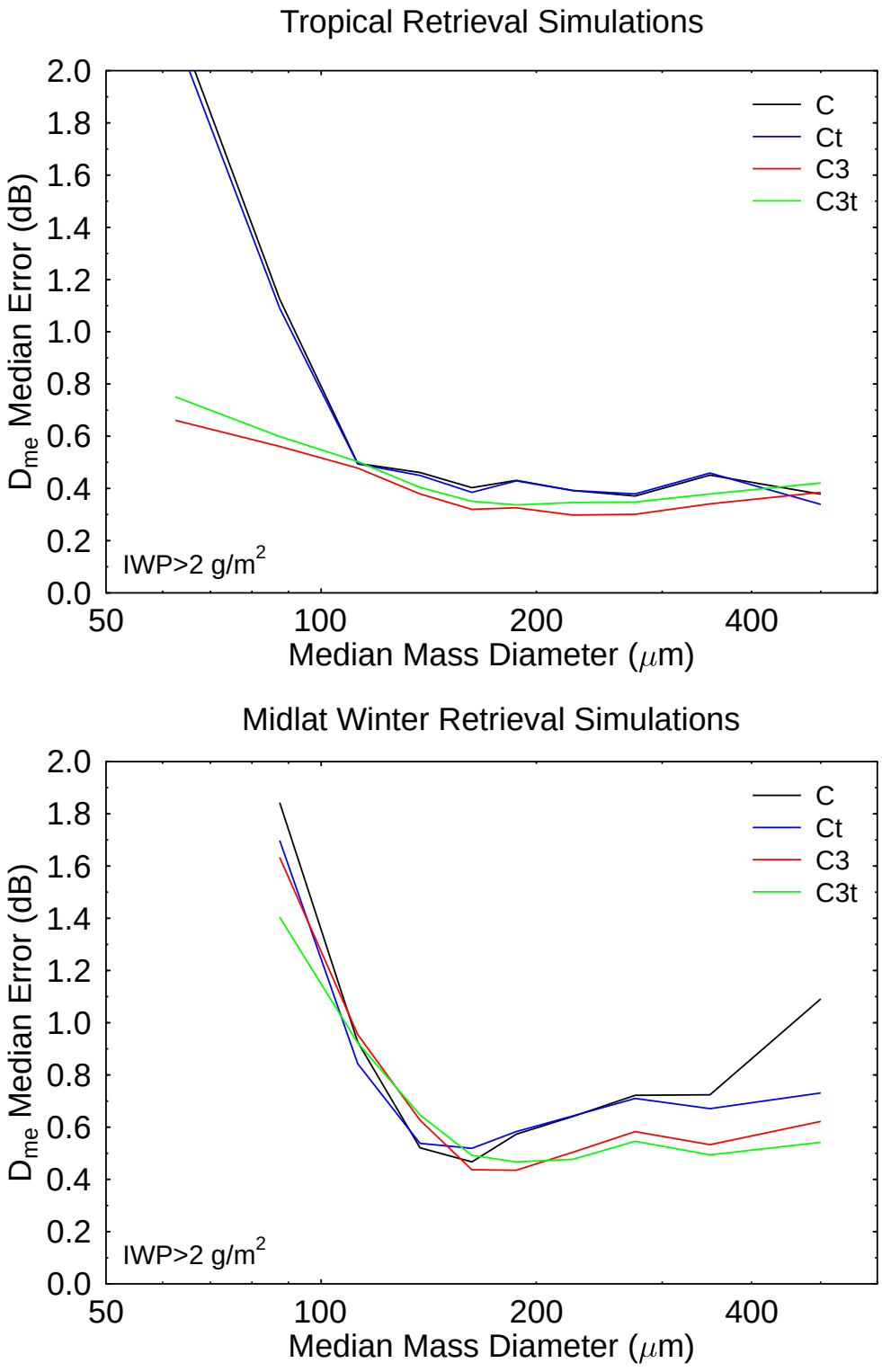
Tropical Retrieval Simulations
2.0
1.8
1.6
1.4
1.2
1.0
0.8
0.6
0.4
0.2
0.0
$D_{me}$ Median Error (dB)
C
Ct
C3
C3t
IWP>2 g/m$^2$
50
100
200
400
Median Mass Diameter ($\mu$m)
Midlat Winter Retrieval Simulations
2.0
1.8
1.6
1.4
1.2
1.0
0.8
0.6
0.4
0.2
0.0
$D_{me}$ Median Error (dB)
C
Ct
C3
C3t
IWP>2 g/m$^2$
50
100
200
400
Median Mass Diameter ($\mu$m)

Figure 9:

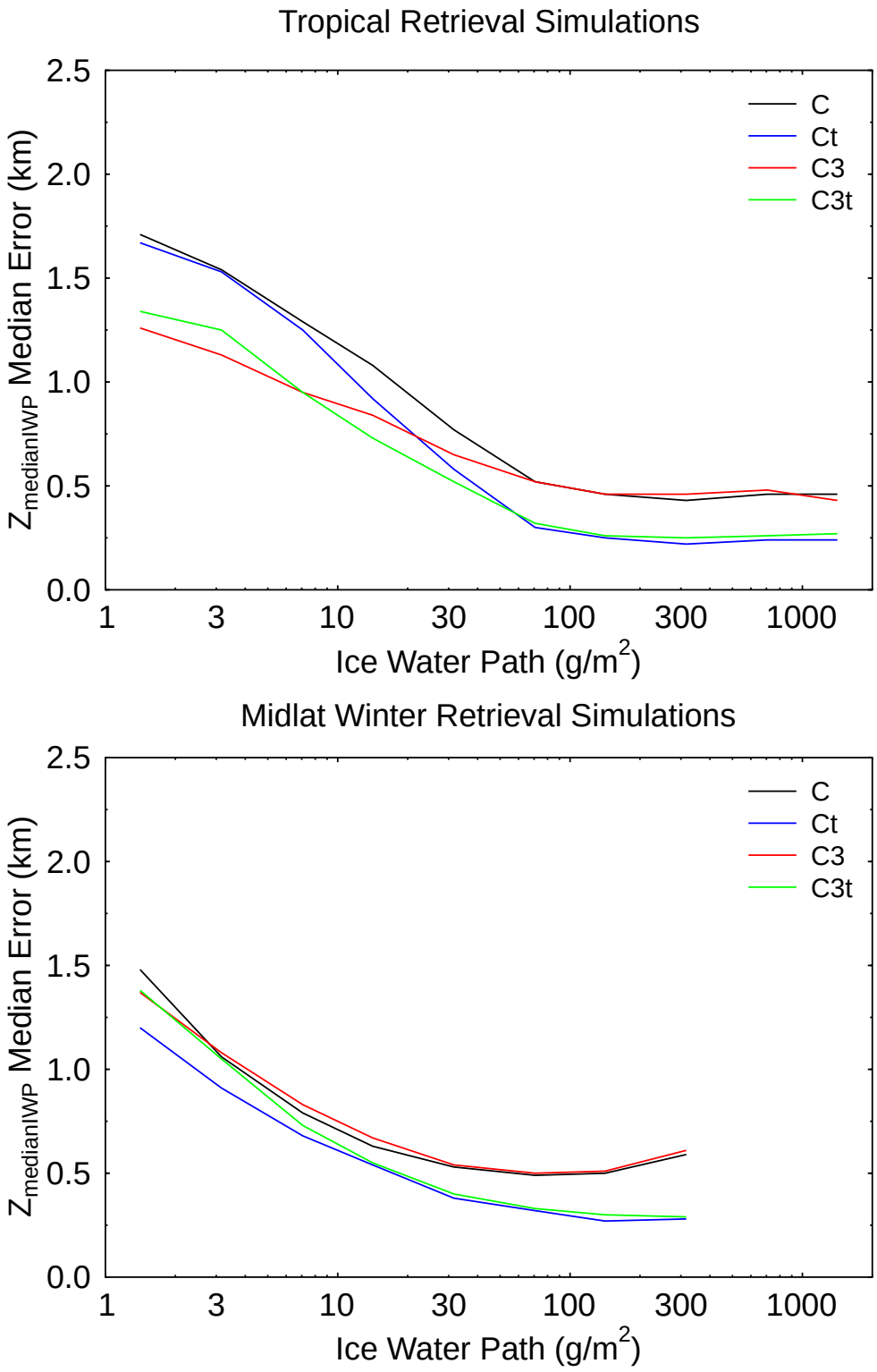
Tropical Retrieval Simulations
2.5
2.0
1.5
1.0
0.5
0.0
$Z_{medianIWP}$ Median Error (km)
1
3
10
30
100
300
1000
Ice Water Path (g/m$^2$)
C
Ct
C3
C3t
Midlat Winter Retrieval Simulations
2.5
2.0
1.5
1.0
0.5
0.0
$Z_{medianIWP}$ Median Error (km)
1
3
10
30
100
300
1000
Ice Water Path (g/m$^2$)
C
Ct
C3
C3t

Figure 10:

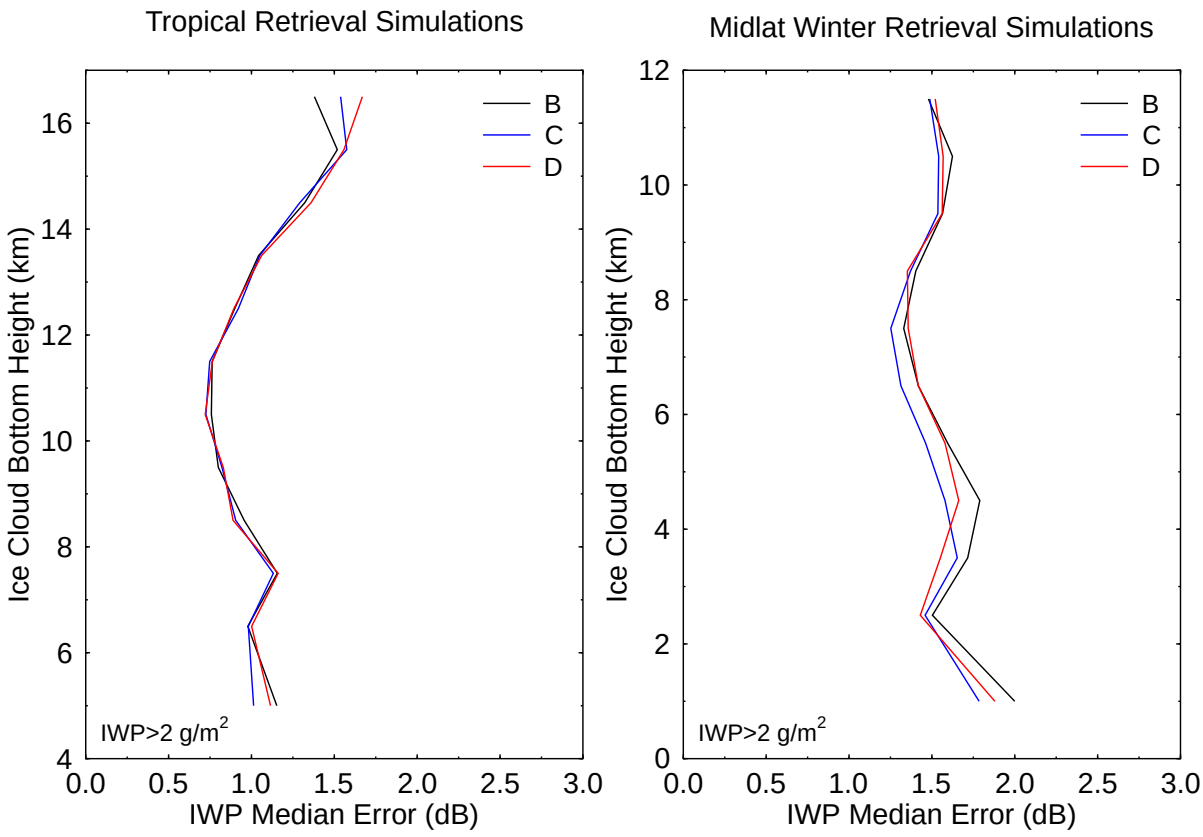


Figure 11:

performance. The reason is that the 183 and 325 GHz weighting functions peak further down into the atmosphere and can sense lower ice clouds. The second set of 448 GHz channels (set D) has a channel with a higher altitude peak, but not one at a lower altitude, which makes the retrieval worse.

How useful are the absorption line channels as compared to using only window channels? Figure 12 compares the C and M sets with and without IR channels. The M set has only window channels except for the 183 GHz receiver. The addition of the water vapor channel at 325 and 448 GHz does significantly improve the IWP retrieval at higher IWP, though the IR channels partially compensate for the removed water vapor channels. The overall results in the tables show that the 325 and 448 GHz channels improve the $D_{me}$ and $Z_{medIWP}$ as well as the IWP and $D_{me}$ accuracy.

Does the exact placement of the window channels matter? One principle for the location of the window channels is to make them equally spaced (in the log) between adjacent channels. Another principle is to maximize the transmission to the midtroposphere. Figure 13 compares the IWP retrieval error for sets C, E, F, G, and H with the IR channels. Sets E and F change the frequency of the 243 GHz channel (to 220 and 280 GHz), while sets G and H change the position of the 664 GHz channel (to 643 and 683 GHz). The results in the figure and tables show that there is not a significant difference between these sets of window channel options.

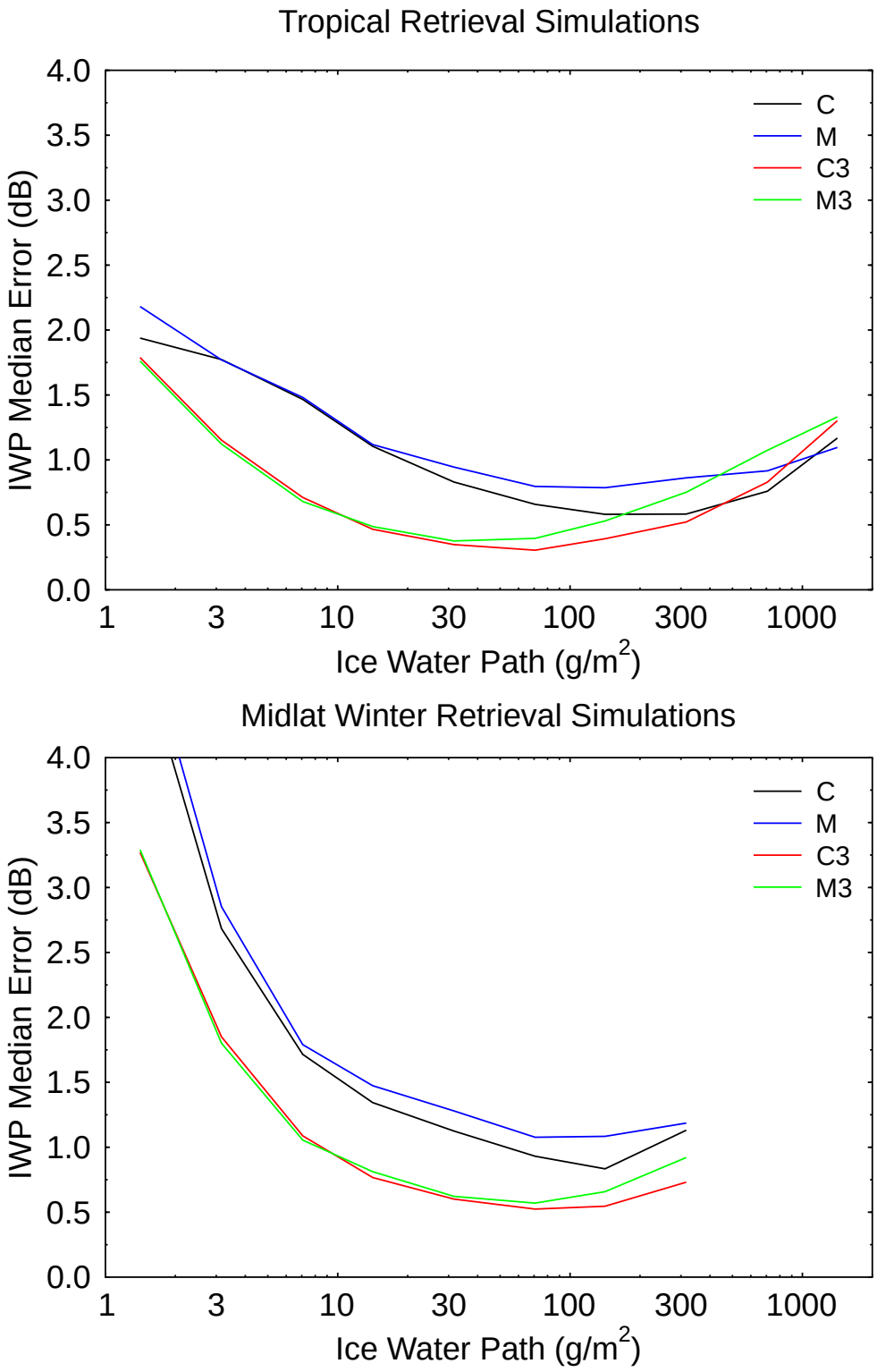
Tropical Retrieval Simulations
IWP Median Error (dB)
Ice Water Path (g/m2)
C
M
C3
M3
0.0
0.5
1.0
1.5
2.0
2.5
3.0
3.5
4.0
1
3
10
30
100
300
1000
Midlat Winter Retrieval Simulations
IWP Median Error (dB)
Ice Water Path (g/m2)
C
M
C3
M3

Figure 12:

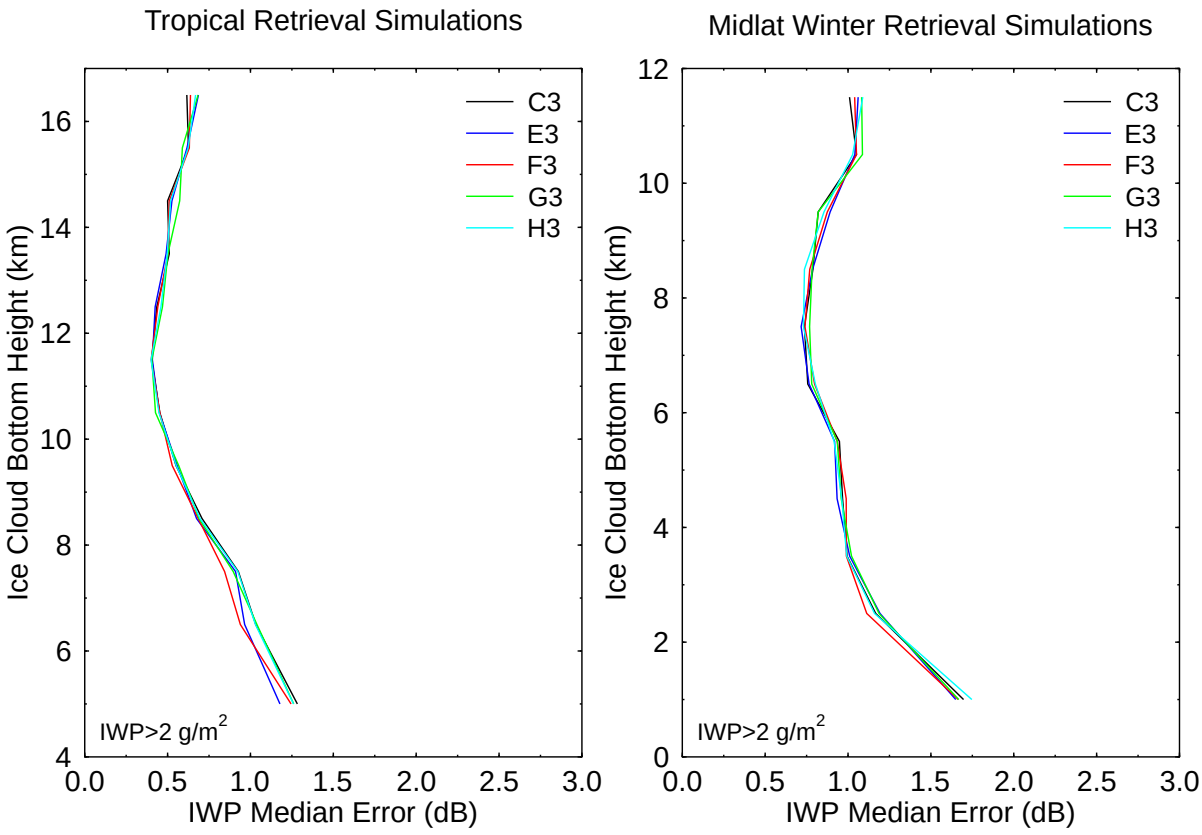
Tropical Retrieval Simulations
Midlat Winter Retrieval Simulations
C3
E3
F3
G3
H3
Ice Cloud Bottom Height (km)
IWP Median Error (dB)
IWP>2 g/m2
0.0
0.5
1.0
1.5
2.0
2.5
3.0
4
6
8
10
12
14
16
0
2
4
6
8
10
12

Figure 13:

Would using absorption line channels for frequencies above 600 GHz improve the ice cloud retrievals? Figure 14 compares the $D_{me}$ accuracy for sets that use the 620 GHz and 916 GHz water lines and the 834 GHz oxygen line. Sets J and K with the 916 GHz channels clearly improve the $D_{me}$ retrievals for the small particles at the higher altitudes of the tropical simulation. This improvement is probably related to the higher frequency of 916 GHz compared to 874 GHz, rather than the use of an absorption line. However, this small particle improvement is negated with the addition of the IR channels, as shown in the figure. Fig. 15 and Table 7 show that there is a significant improvement in IWP retrieval accuracy for the midlatitude winter simulation from using the 620 GHz water vapor line (set I compared to set C). There is no indication that using the narrow oxygen line at 834 GHz improves the retrievals.

Would it be better to use other midrange submillimeter absorption lines, such as the oxygen lines at 425 and 487 GHz or the water vapor line at 380 GHz? Figure 16 compares the IWP retrieval accuracy for sets C, N, O, and P with the IR channels included. The midlatitude winter simulation shows that the 380 GHz channels (sets N and O) are not a good substitute for the 325 GHz channels, probably because the lowest 325 GHz weighting function peaks lower in the atmosphere than the lowest 380 GHz weighting function. The oxygen line channels in sets N5 and O5 do not appear to offer any advantages for IWP or $D_{me}$ retrievals. The 425 GHz channels of set P, however, do improve the $Z_{medIWP}$ accuracy (see Fig. 17), though this advantage is negated if temperature profile information is available from NWP models. Set P also improves the IWP accuracy for the midlatitude winter simulation, probably because the 425 GHz channels have weighting functions that peak lower than those of the 448 GHz channels.

The results in Table 8 show that the IR channel set 5, with 6.7, 8.5, and 12.0 $\mu$m is the best IR set. Figure 18 shows the difference between the IR sets for particle size retrievals. There is little difference in the midlatitude simulation because it doesn't have the smallest particles, but in the tropical simulation sets C3 and C5 have substantial smaller $D_{me}$ errors than the others for small particles. The difference for IWP retrievals is much less dramatic and there is only a small difference between the five IR channel sets. Figure 19 shows that there is a large difference in $Z_{medIWP}$ retrieval accuracy between the IR channel sets for high altitude tropical cirrus which has small particles. In the graphs IR channel sets 3 and 5 appear rather similiar.

The water vapor retrieval error is summarized in Fig. 20. Compared to the natural variability of water vapor the retrievals with only microwave channels (set C) are poor (same for microwave combined with infrared channels; not shown). In the tropical case the fractional retrieval errors are relatively low, but so is the natural variability (see the relative humidity profile statistics in Fig. 6). The addition of temperature information in the form of the oxygen line microwave channels in set P noticeably improves the retrievals for upper layers in the tropical simulation. A very substantial reduction in water vapor retrieval error is obtained by the addition of the five layer temperature profile information (set Ct). The addition of three infrared channels (set C3t) actually slightly degrades the retrieval accuracy (an example of the finite database problem). The fractional rms water vapor retrieval accuracy with the temperature profile information is about 0.2 in the tropical simulation and about 0.3 in the troposphere part of the midlatitude winter simulation (below 8 km).

The microwave radiometer options with less than six receivers are studied in the channel sets A and Q through Z. The first option is to remove the 243 GHz channel (set A) as being too low in frequency to matter for cirrus clouds. Another option is to remove the 874 GHz channel (set Q), which might be necessary if the technology for that receiver proved too difficult. Set R is the combination of both by deleting 243 and 874 GHz receivers. Figure 21 shows the IWP retrieval

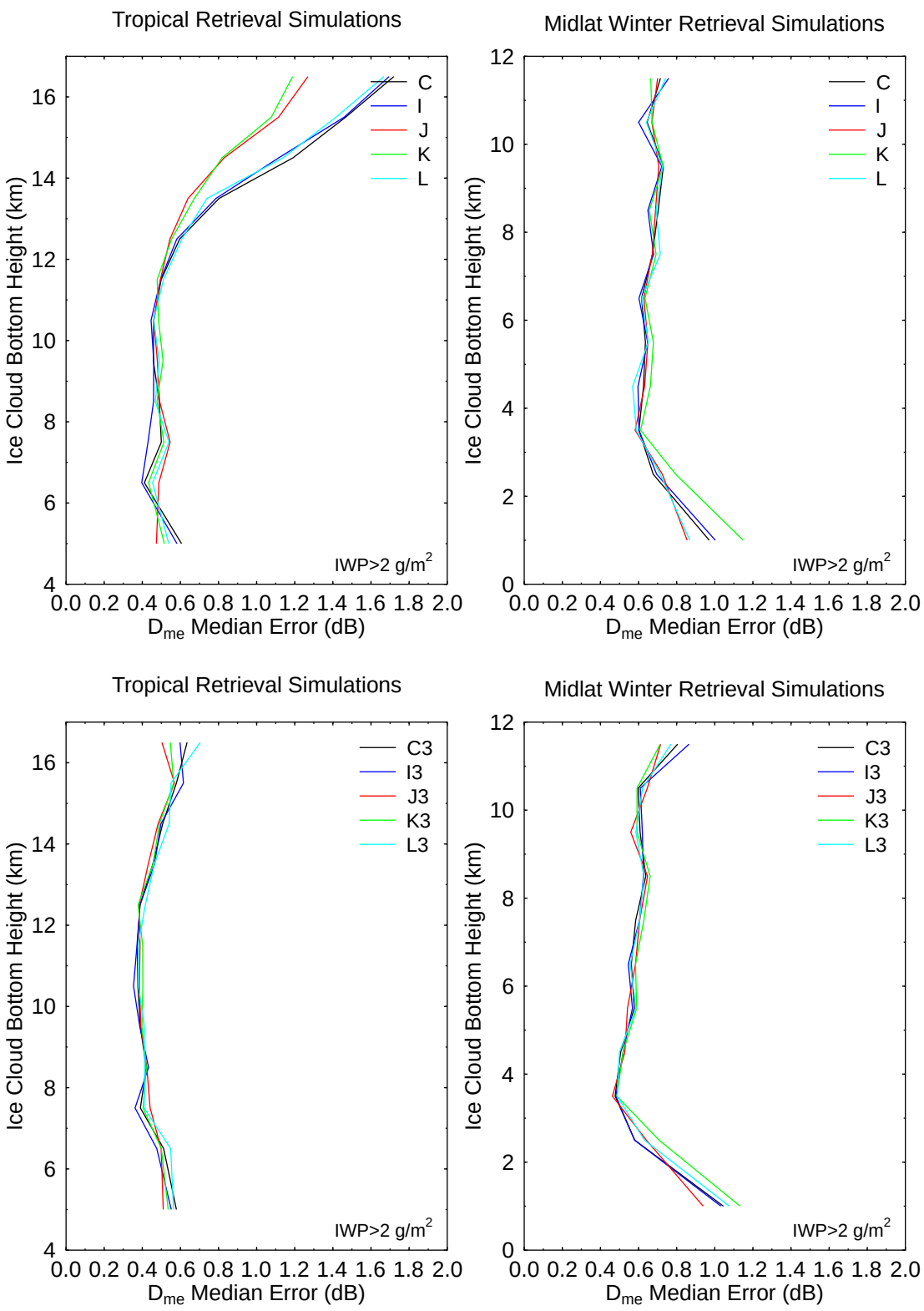
Tropical Retrieval Simulations
Midlat Winter Retrieval Simulations
Ice Cloud Bottom Height (km)
D_me Median Error (dB)
IWP>2 g/m^2
C
I
J
K
L
C3
I3
J3
K3
L3

Figure 14:

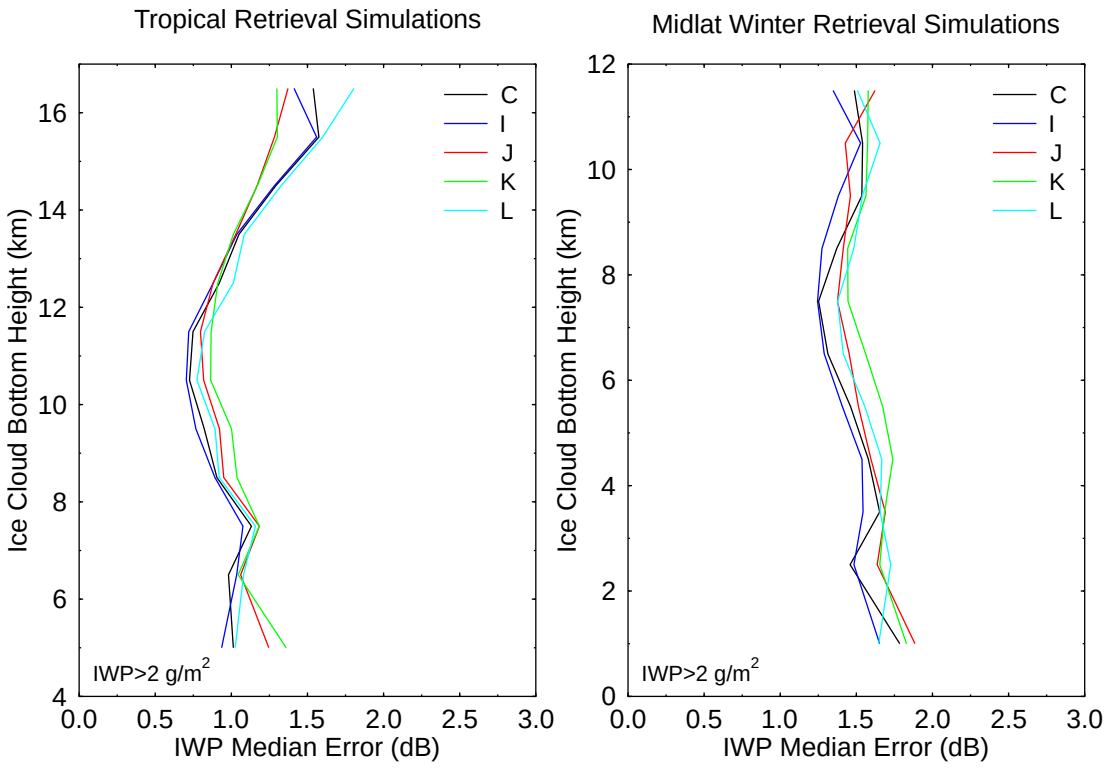
Tropical Retrieval Simulations
Midlat Winter Retrieval Simulations
Ice Cloud Bottom Height (km)
IWP Median Error (dB)
IWP>2 g/m2
C
I
J
K
L
0.0
0.5
1.0
1.5
2.0
2.5
3.0
4
6
8
10
12
14
16
0
2
4
6
8
10
12

Figure 15:

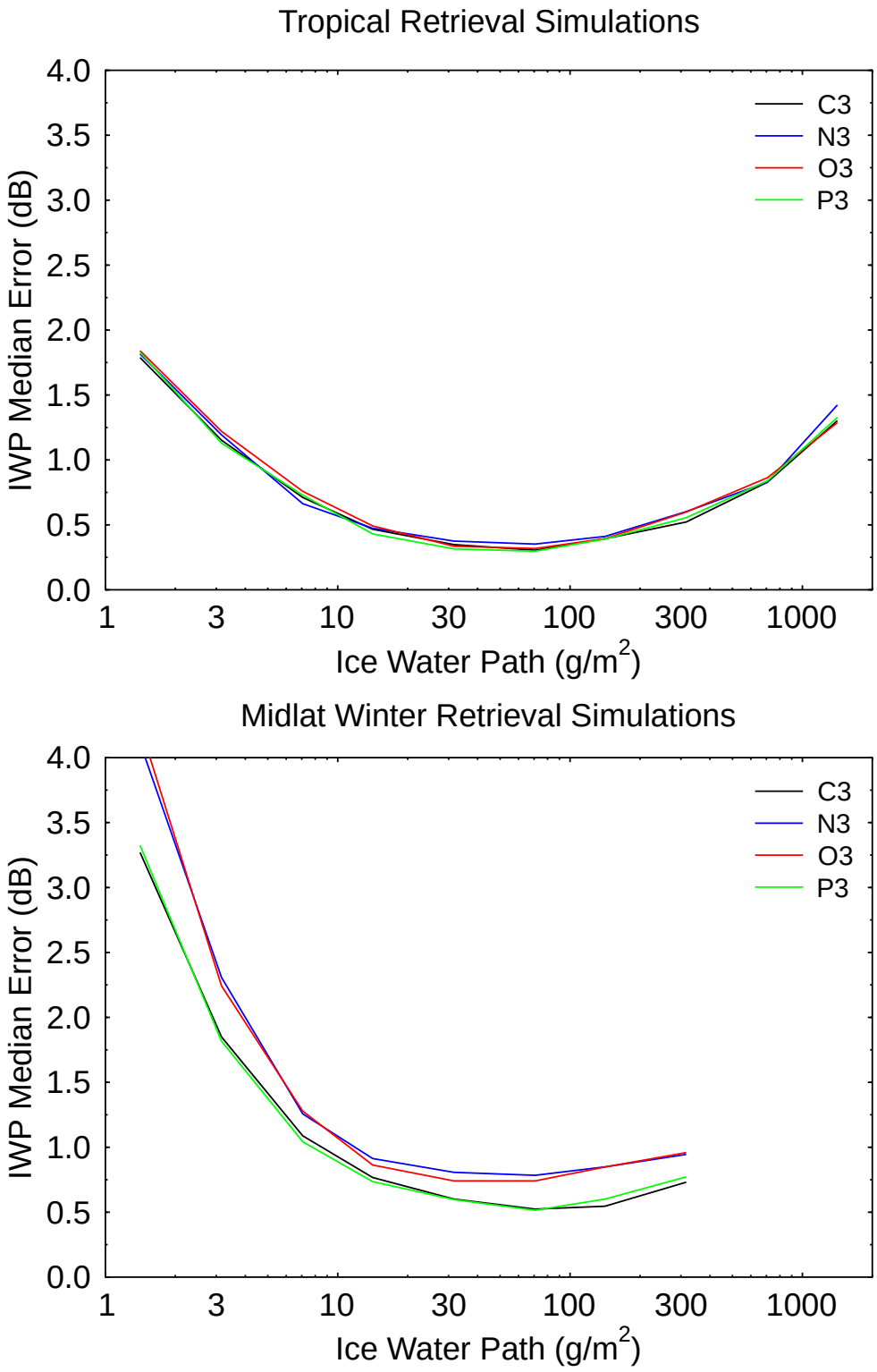
Tropical Retrieval Simulations
IWP Median Error (dB)
4.0
3.5
3.0
2.5
2.0
1.5
1.0
0.5
0.0
1
3
10
30
100
300
1000
Ice Water Path (g/m2)
C3
N3
O3
P3
Midlat Winter Retrieval Simulations
IWP Median Error (dB)
4.0
3.5
3.0
2.5
2.0
1.5
1.0
0.5
0.0
1
3
10
30
100
300
1000
Ice Water Path (g/m2)
C3
N3
O3
P3

Figure 16:

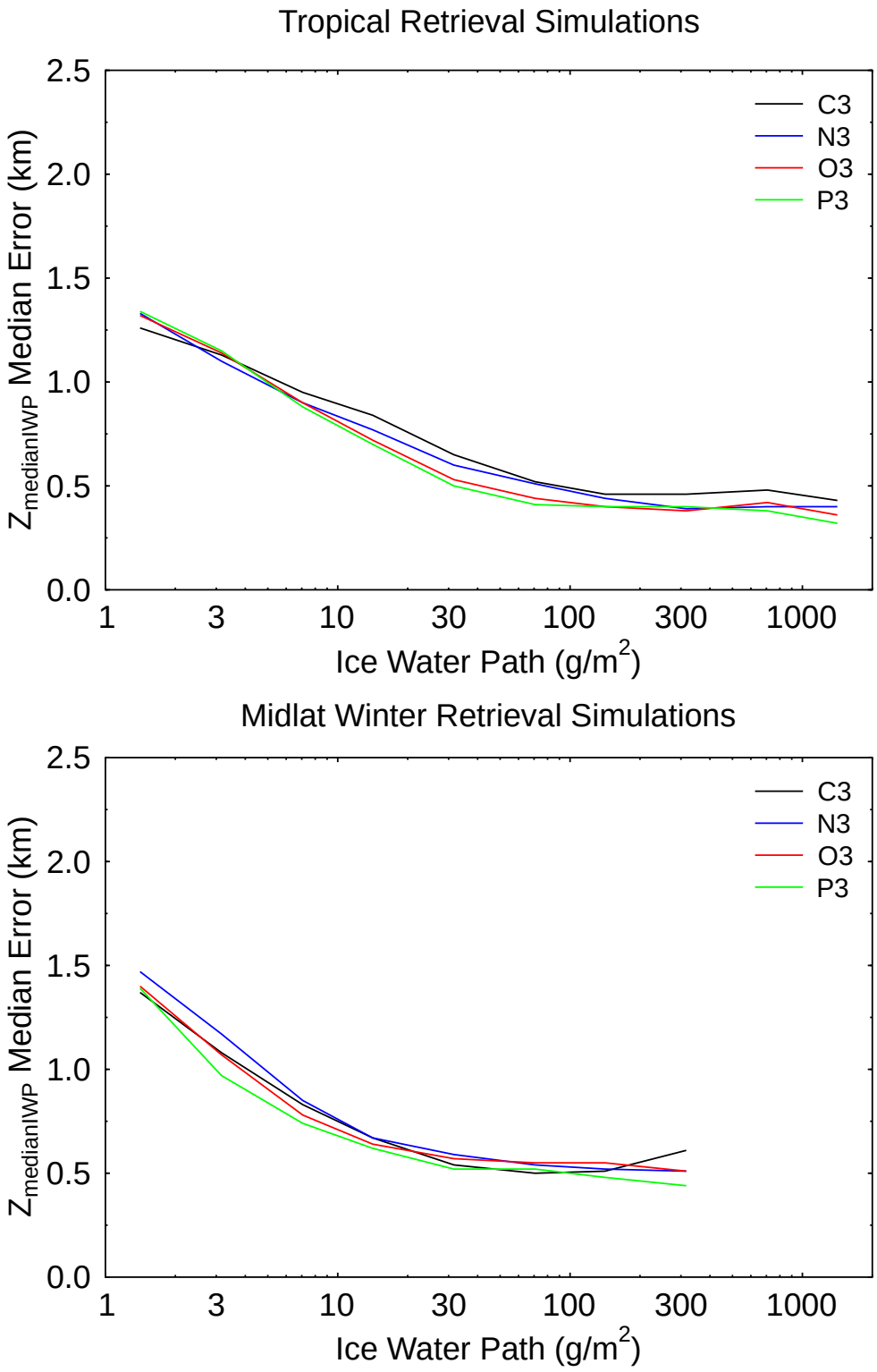
Tropical Retrieval Simulations
2.5
2.0
1.5
1.0
0.5
0.0
$Z_{medianIWP}$ Median Error (km)
C3
N3
O3
P3
1
3
10
30
100
300
1000
Ice Water Path (g/m$^2$)
Midlat Winter Retrieval Simulations
2.5
2.0
1.5
1.0
0.5
0.0
$Z_{medianIWP}$ Median Error (km)
C3
N3
O3
P3
1
3
10
30
100
300
1000
Ice Water Path (g/m$^2$)

Figure 17:

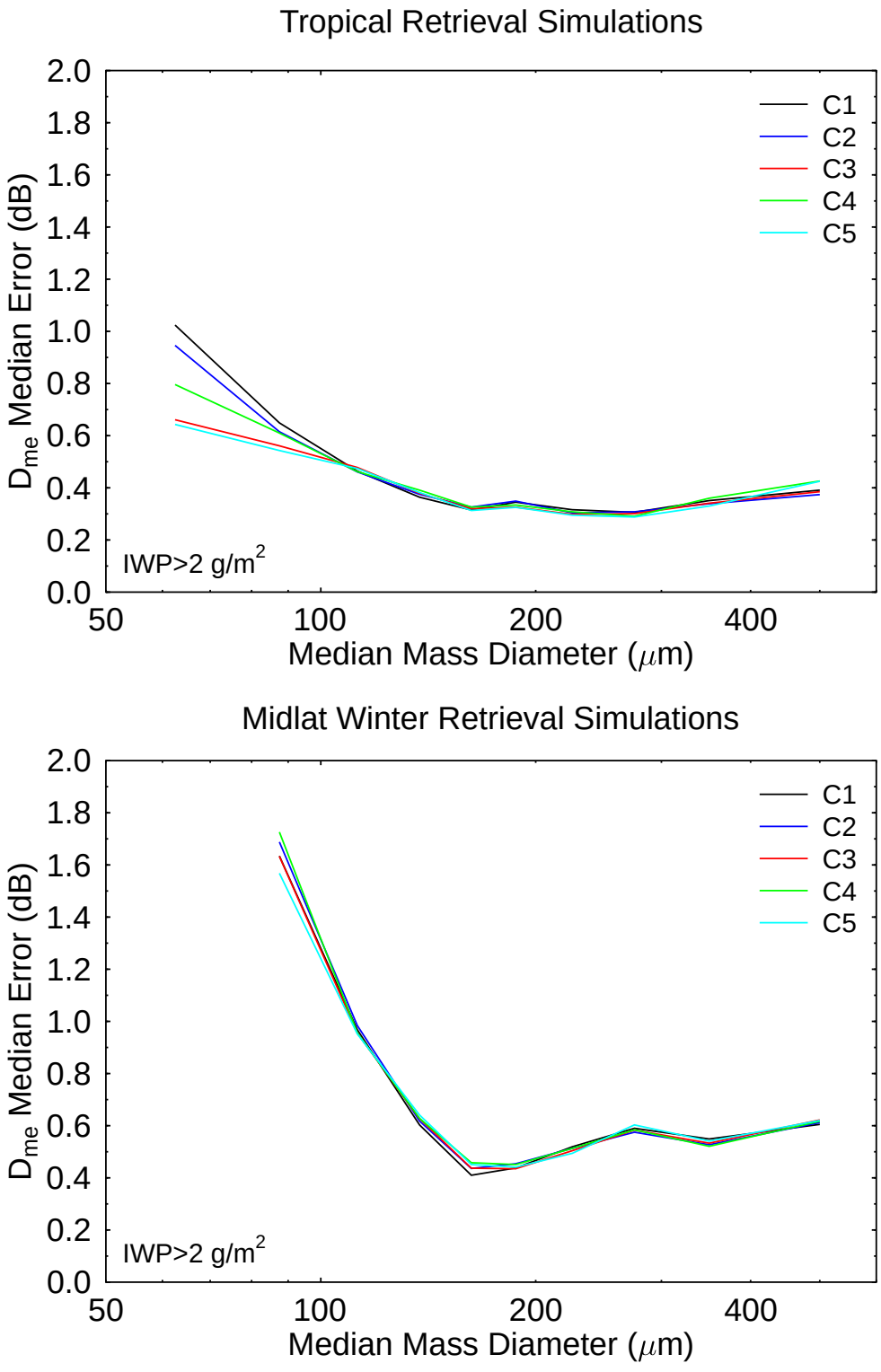
Tropical Retrieval Simulations
2.0
1.8
1.6
1.4
1.2
1.0
0.8
0.6
0.4
0.2
0.0
$D_{me}$ Median Error (dB)
C1
C2
C3
C4
C5
IWP>2 g/m$^2$
50
100
200
400
Median Mass Diameter ($\mu$m)
Midlat Winter Retrieval Simulations
2.0
1.8
1.6
1.4
1.2
1.0
0.8
0.6
0.4
0.2
0.0
$D_{me}$ Median Error (dB)
C1
C2
C3
C4
C5
IWP>2 g/m$^2$
50
100
200
400
Median Mass Diameter ($\mu$m)

Figure 18:

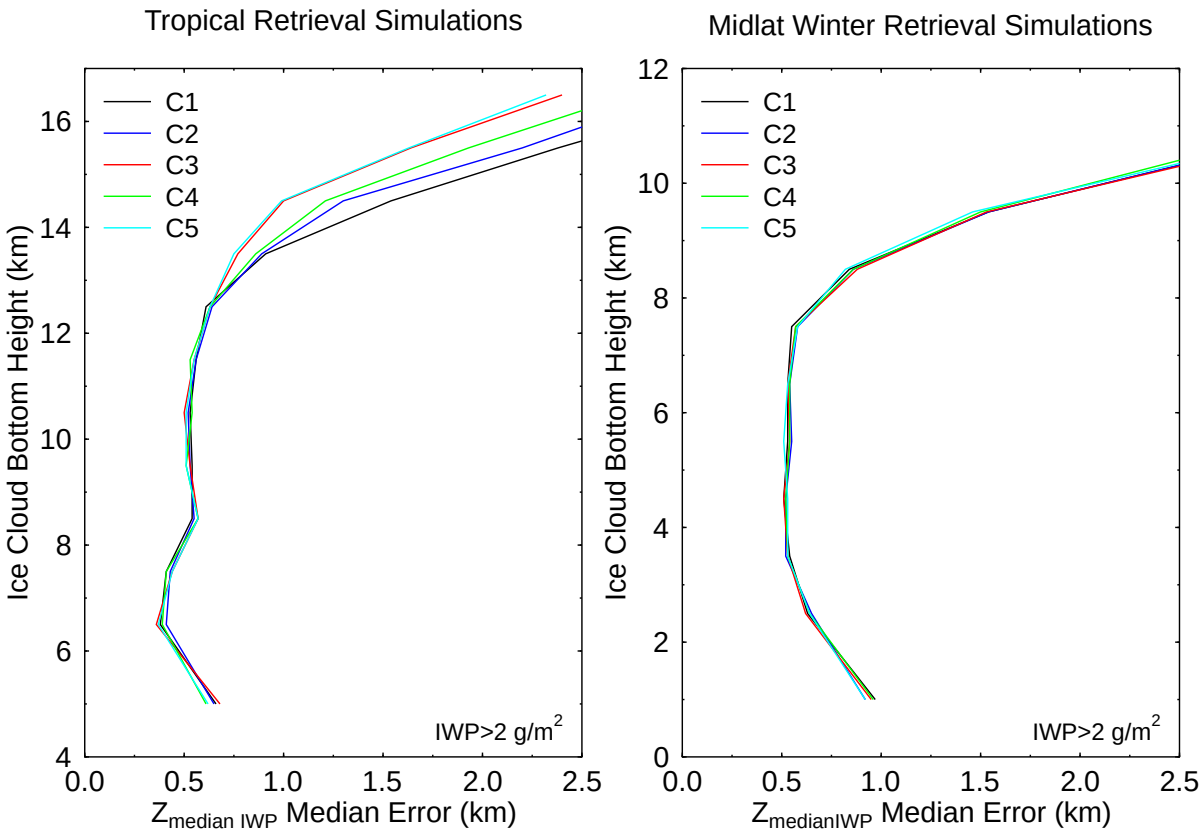
Tropical Retrieval Simulations
Midlat Winter Retrieval Simulations
C1
C2
C3
C4
C5
IWP>2 g/m2
Ice Cloud Bottom Height (km)
Z median IWP Median Error (km)
Z medianIWP Median Error (km)

Figure 19:

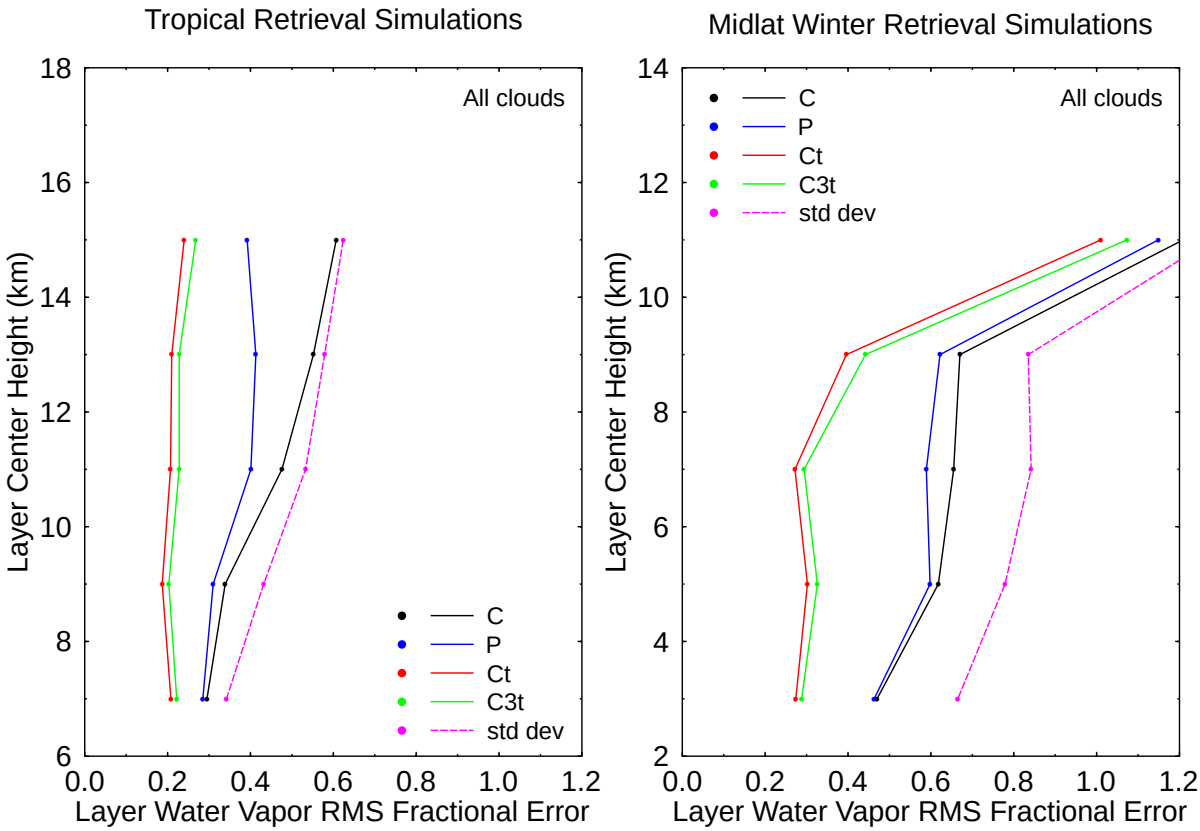


Figure 20: Fractional rms water vapor retrieval error for the five layers. The ratio of the standard deviation of water vapor amount to the mean is shown to compare the retrieval error to the natural variability.

accuracy as a function of $D_{me}$ for sets A, C, Q, and R without the IR channels. The 874 GHz channel is clearly important for small particles, though the IR channels can partially compensate for its loss (not shown). The 243 GHz channel is important to IWP accuracy for $D_{me} > 400$ $\mu$m.

The sets with four microwave receivers, R through W including the IR channels, are compared in Fig. 22. Set S with the 874 GHz channel is clearly superior to the others because of its better sensitivity to small particles (it is the only one that has a 874 GHz receiver). Table 8 indicates that sets R, S, and W are the best in general for IWP and $D_{me}$ retrievals, but S is preferred due to its better accuracy for small particles. The superiority of set S is even more clear with the infrared channels (see Table 8).

Figure 23 compares IWP retrieval error of the three microwave sets with three receivers (X, Y, Z) to the standard set C. Set X with 183, 325, and 448 GHz receivers is clearly the best for the midlatitude winter simulation, which does not have the smallest ice particles, however, it is the worst of the three for the tropical simulation. Set Z has considerably lower IWP retrieval error for the tropical simulation, but it highest for the midlatitude winter case. So there is not a clear choice for the albeit small number of three receiver options studied here.

## 7. Polarized Radiative Transfer Simulations

The fast Eddington second approximation radiative transfer algorithm used to generate the retrieval and testing databases above is unpolarized and therefore not suited for studying horizontally oriented particles with large polarization signatures. Ultimately, a fast polarized Eddington radiative transfer algorithm should be implemented for the retrieval method. For this report the approach taken was to implement a fully polarized multistream doubling-adding radiative transfer model (Evans and Stephens, 1991) in the database generation program.

The multistream polarized model performs radiative transfer with thermal radiation sources in media with particles that may have preferred orientation in zenith angle but are randomly oriented in azimuth. The single scattering properties are input as $2 \times 2$ Stokes scattering matrices depending on incident and outgoing discrete zenith angles, $2 \times 2$ Stokes extinction matrices depending on incident zenith angle, and Stokes emission vectors depending on incident zenith angle. For the calculations shown below 8 Gaussian quadrature zenith angles are used per hemisphere (i.e. 16 total). The single scattering information input to the multistream polarized model is thus much larger than the single extinction, single scattering albedo, and asymmetry parameter that the Eddington model requires for a calculation. The doubling algorithm is used to compute the reflection and transmission matrices and source vectors for homogeneous layers from the single scattering properties (e.g. see Evans and Stephens, 1991). Special routines are used to speed the generation of the reflection and transmission matrices for nonscattering layers (i.e. with only molecular absorption) and for the combination (adding) of the properties of adjacent layers if one or both is nonscattering. The output radiance may be calculated at the interface of any computational layer. The output radiance at the desired zenith angle is linearly interpolated between the radiances at the quadrature angles calculated by the doubling-adding model. The polarized radiative transfer model may be run using a single Stokes parameter ($I$) or two Stokes parameters ($I$ and $Q$) depending on whether polarized output is required. The other two Stokes parameters ($Q$ and $V$) are zero for azimuthally symmetric media, assuming the azimuthally dependent polarization from the ocean surface can be ignored due to the high water vapor opacity. For each channel the output may be chosen to be

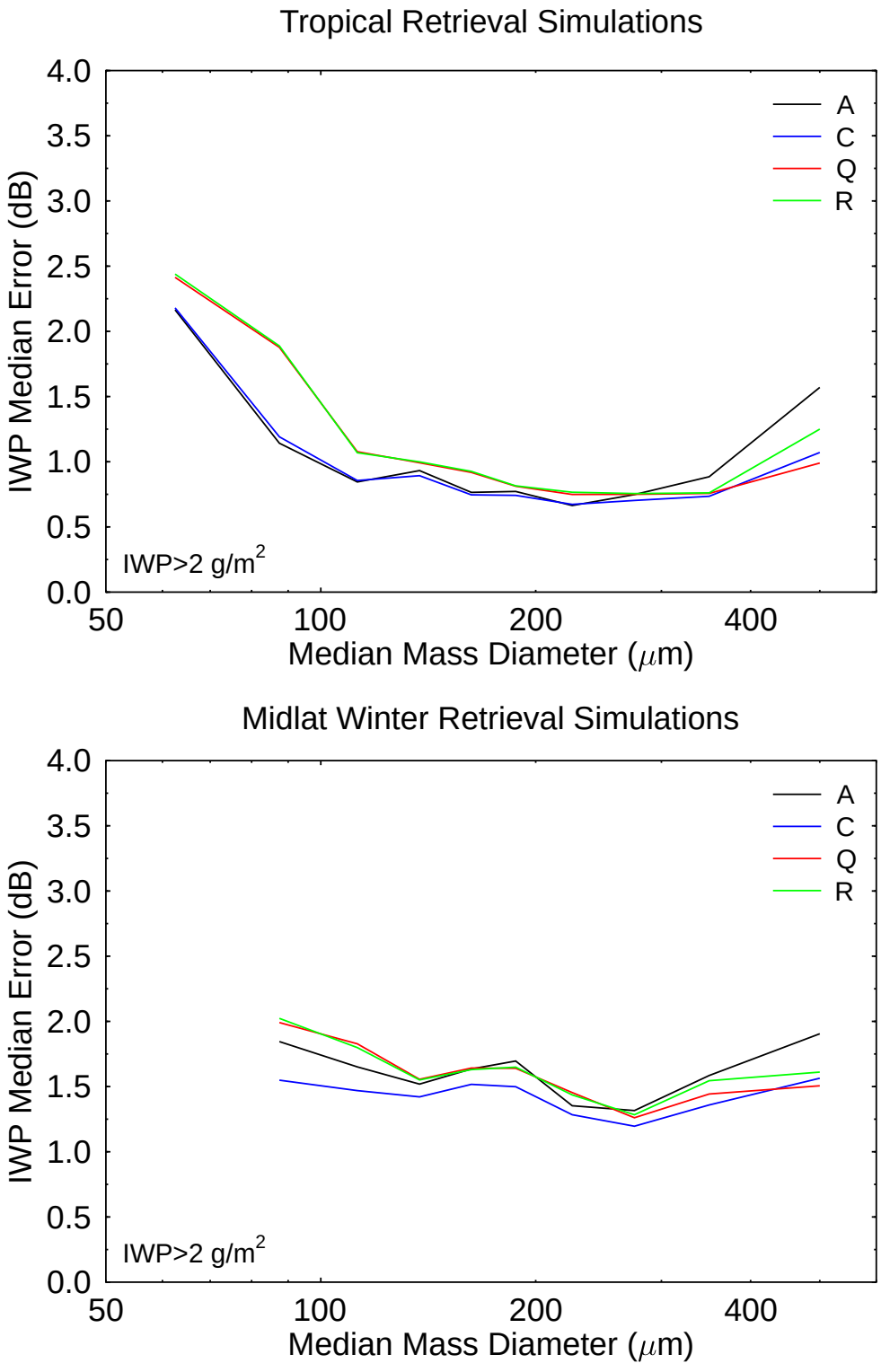
Tropical Retrieval Simulations
IWP Median Error (dB)
4.0
3.5
3.0
2.5
2.0
1.5
1.0
0.5
0.0
A
C
Q
R
IWP>2 g/m2
50
100
200
400
Median Mass Diameter (μm)
Midlat Winter Retrieval Simulations
IWP Median Error (dB)
4.0
3.5
3.0
2.5
2.0
1.5
1.0
0.5
0.0
A
C
Q
R
IWP>2 g/m2
50
100
200
400
Median Mass Diameter (μm)

Figure 21:

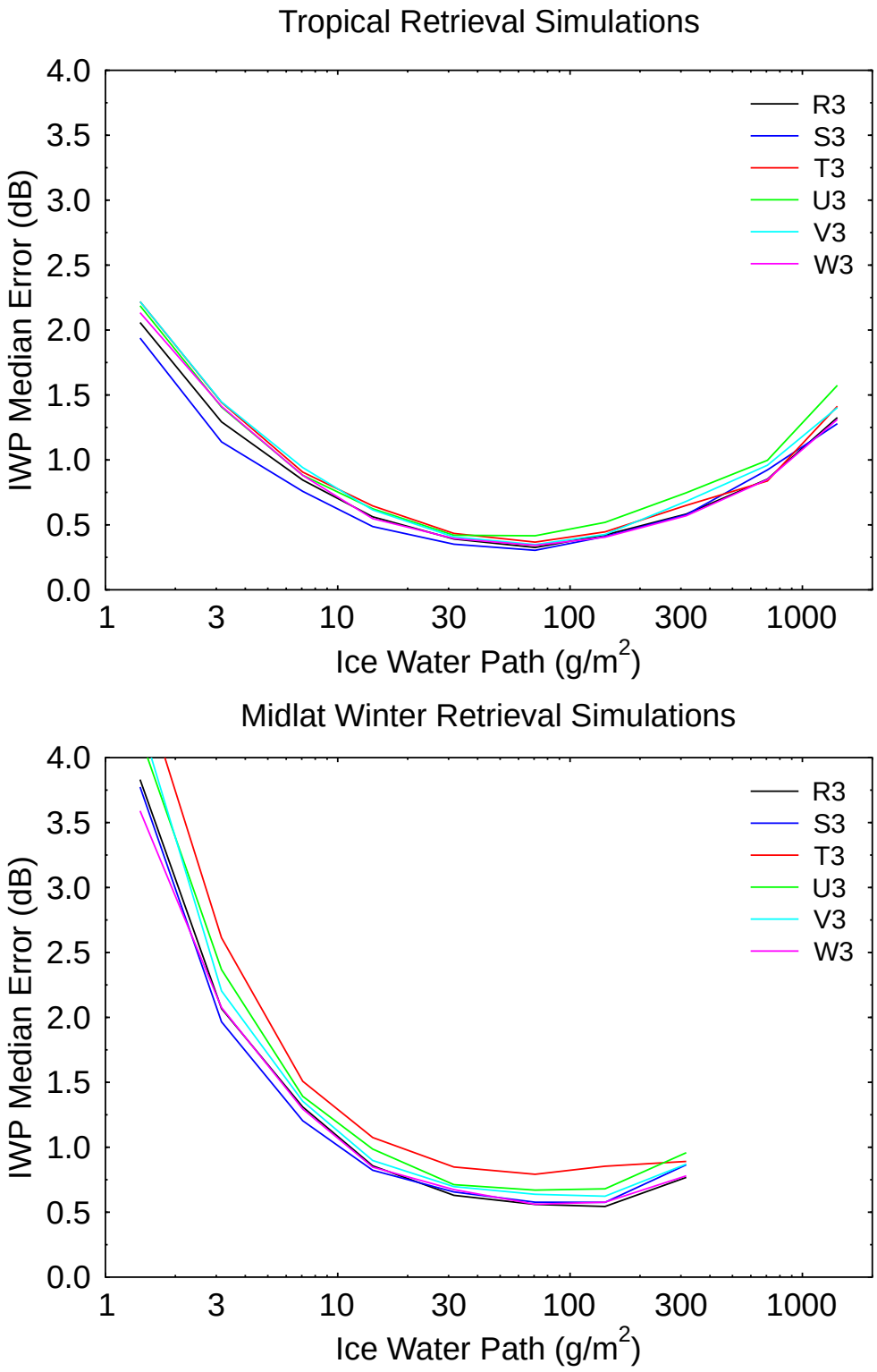
Tropical Retrieval Simulations
IWP Median Error (dB)
4.0
3.5
3.0
2.5
2.0
1.5
1.0
0.5
0.0
1
3
10
30
100
300
1000
Ice Water Path (g/m2)
R3
S3
T3
U3
V3
W3
Midlat Winter Retrieval Simulations
IWP Median Error (dB)
4.0
3.5
3.0
2.5
2.0
1.5
1.0
0.5
0.0
1
3
10
30
100
300
1000
Ice Water Path (g/m2)
R3
S3
T3
U3
V3
W3

Figure 22:

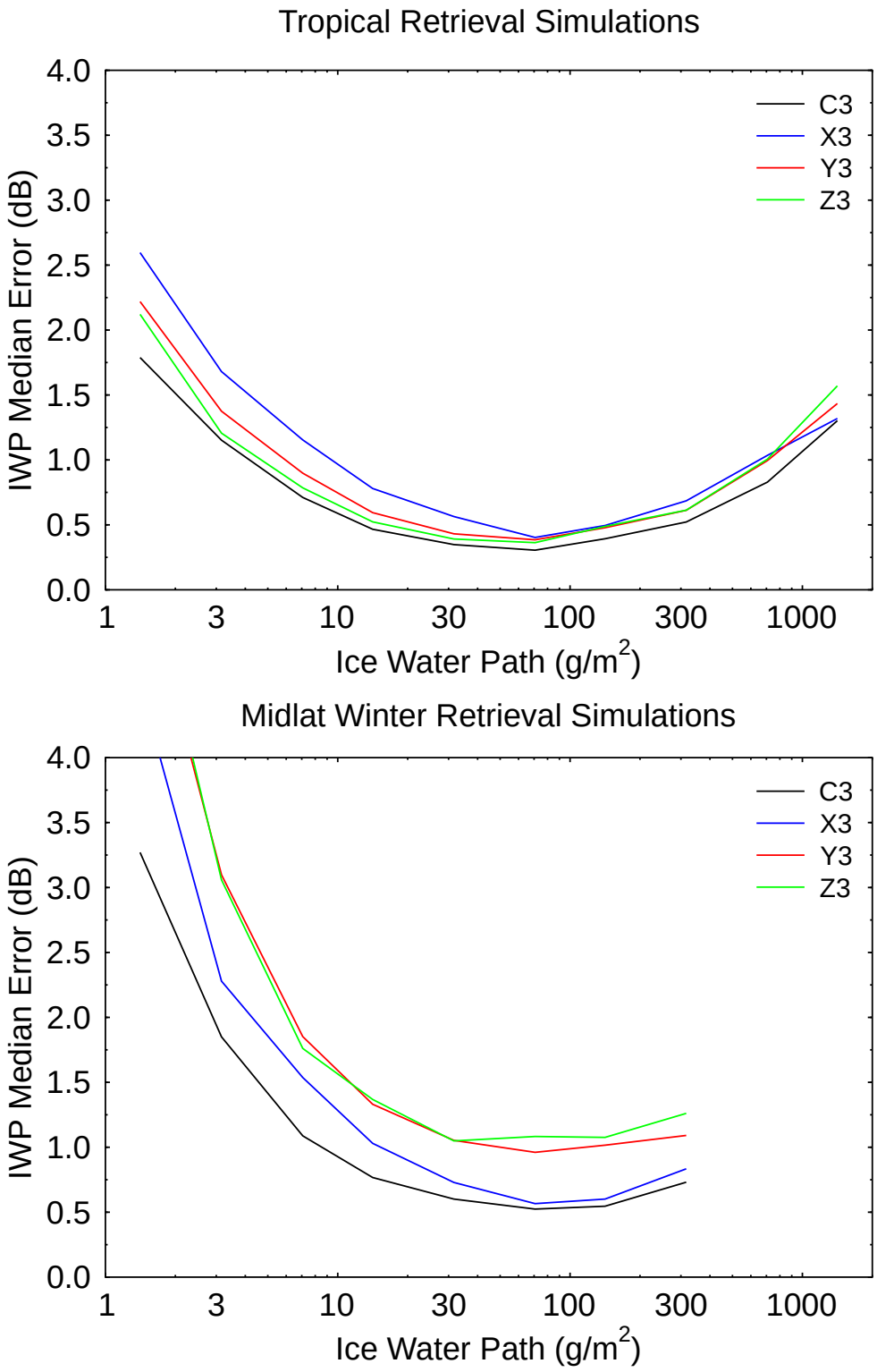
Tropical Retrieval Simulations
IWP Median Error (dB)
4.0
3.5
3.0
2.5
2.0
1.5
1.0
0.5
0.0
1
3
10
30
100
300
1000
Ice Water Path (g/m2)
C3
X3
Y3
Z3
Midlat Winter Retrieval Simulations
IWP Median Error (dB)
4.0
3.5
3.0
2.5
2.0
1.5
1.0
0.5
0.0
1
3
10
30
100
300
1000
Ice Water Path (g/m2)
C3
X3
Y3
Z3

Figure 23:

unpolarized, vertically polarized, or horizontally polarized brightness temperature or unpolarized radiance (units of mW $m^{-2}$ $st^{-1}$cm).

The single scattering properties input to the polarized multistream version of the database generation program are computed with the discrete dipole approximation (DDA) for horizontally oriented or randomly oriented particles (see Evans et al., 1998 and references therein). Since the goal here is to determine the maximum range of microwave polarization from ice crystals, only two particle shapes are considered: horizontally oriented solid columns and randomly oriented 7-bullet rosettes. The aspect ratios of the columns and bullets are from Yang et al. (2000). The DDA code calculates the scattering properties for individual ice crystals with maximum diameters from 10 $\mu$m to 2500 $\mu$m (in 0.5 dB steps), and these properties are then assembled into gamma size distributions with a range of $D_{me}$ (from 25 $\mu$m to 400 $\mu$m ) and two distribution widths ($\alpha = 0$ and $\alpha = 2$). The scattering properties are calculated at the receiver center frequencies (and 150 and 999 GHz) and interpolated in frequency and in $D_{me}$.

The multistream radiative transfer version of the database generation program is first run in unpolarized mode on bullet rosette clouds to determine the error due to the Eddington approximation in the original version. The testing databases with 10,000 cases are computed for the "C" microwave set of channels for the tropical and midlatitude winter simulations with both the Eddington and multistream radiative transfer codes. Table 9 lists the mean and rms difference in brightness temperature between the Eddington and multistream radiative transfer models for each channel. The Eddington rms error for the window channels increases with frequency, though it only reaches about 1.0 K. The bias is small for the tropical simulation but becomes more negative with frequency for the midlatitude winter simulation. The error increases with IWP (not shown) with the maximum error envelope range at 874 GHz of -3 to +5 K for the tropical simulation and -3 to 0 K for the midlatitude winter simulation. Overall, the Eddington model is surprisingly accurate considering its simplicity. The systematic uncertainty assumed in the retrieval modeling of 1 K (due to instrument calibration and radiative transfer modeling) seems appropriate, though perhaps it should depend on frequency and IWP.

The next calculation with the polarized multistream model is to illustrate the range of brightness temperature polarization that could be expected. The vertical and horizontal brightness temperature at 664 GHz and 874 GHz are computed for horizontally oriented columns and randomly oriented rosettes for 1000 cases from the tropical and midlatitude simulations. Figures 24 and 25 show the polarized brightness temperature difference as a function of ice water path. As expected, the maximum polarization difference is much higher for columns than for rosettes, though the polarization difference for rosettes ranges up to 4 K. The polarization difference for columns reaches about 24 K at 874 GHz and about 30 K at 664 GHz for IWP above 100 g/$m^2$ in the tropical simulation. There is a large range in polarization difference for a single IWP due to the effect of particle size, water vapor absorption, and multiple scattering on polarization. The decrease in the maximum polarization difference for IWP above 200 g/$m^2$, which can be seen clearly in Fig. 24, is probably due to multiple scattering. Real clouds with mixtures of particles would be expected to have polarized brightness temperature differences between that of the rosettes and columns shown here.

With this large effect of particle shape on polarization, how does particle shape affect the ice cloud retrieval accuracy simulated earlier? Given the large difference between horizontal and vertical polarization for columns, which is the best polarization to use for those instrument frequencies having only one polarization? These questions are addressed by performing retrievals on simu-

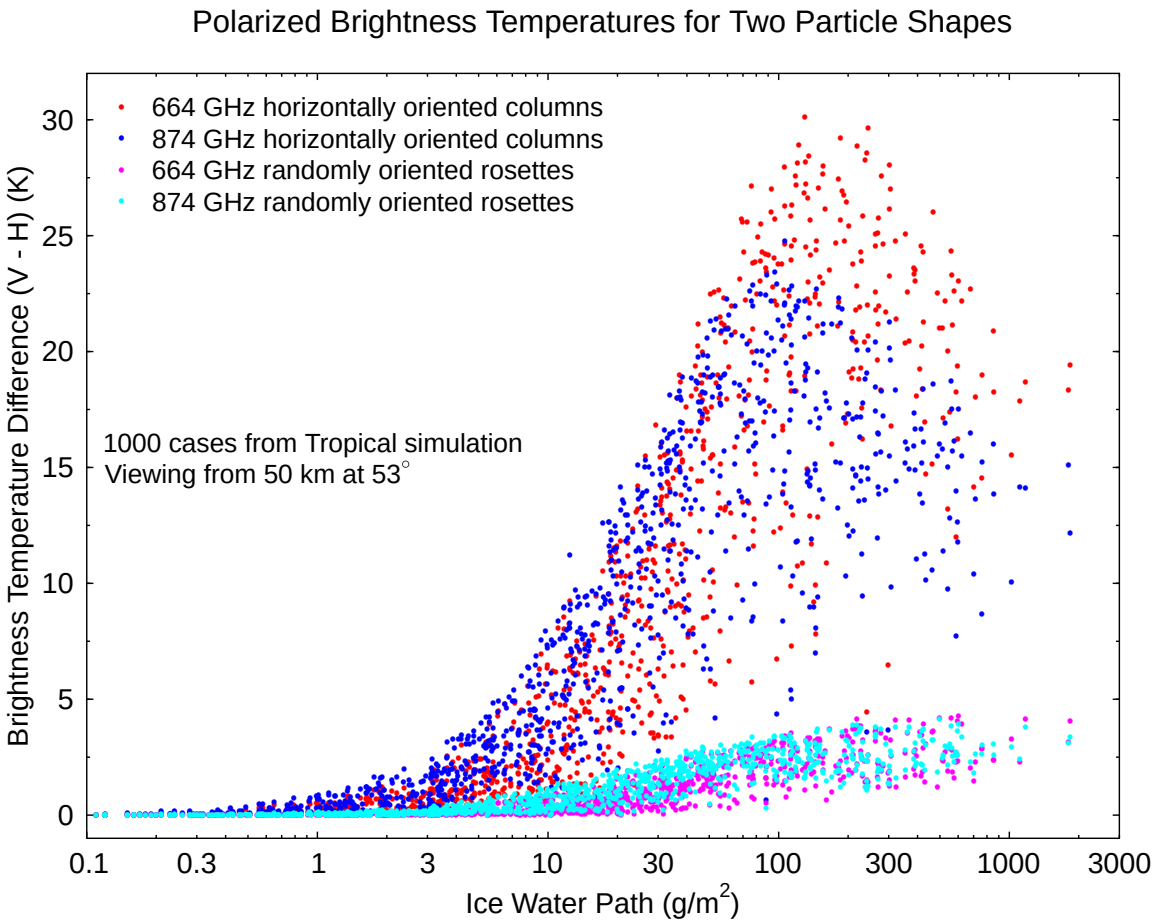


Figure 24: The difference between vertical and horizontal polarized brightness temperature for two particle shapes at two frequencies for the tropical simulation.

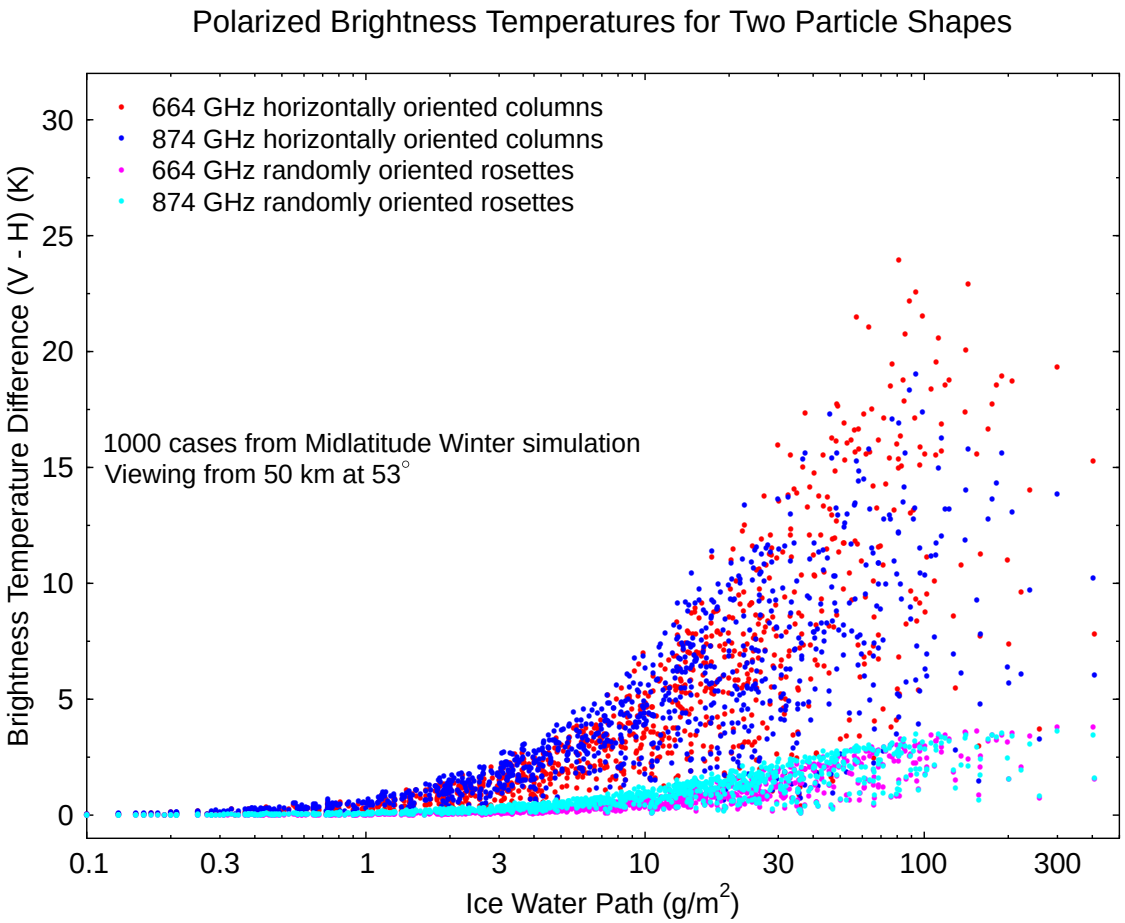


Figure 25: The difference between vertical and horizontal polarized brightness temperature for two particle shapes at two frequencies for the midlatitude winter simulation.

Table 9: Statistics of brightness temperature differences (K) between Eddington and multistream radiative transfer models for the microwave channels in set C for the two simulations.

| | Tropical | | Midlat Winter | |
|---|---|---|---|---|
| Frequency | mean | rms | mean | rms |
| 183.3±1.5 | 0.00 | 0.18 | 0.01 | 0.07 |
| 183.3±3.5 | 0.05 | 0.23 | 0.03 | 0.09 |
| 183.3±7.0 | 0.12 | 0.33 | 0.09 | 0.12 |
| 243.2±2.5 | 0.19 | 0.55 | 0.01 | 0.19 |
| 325.1±1.5 | -0.08 | 0.45 | -0.10 | 0.27 |
| 325.1±3.5 | 0.06 | 0.53 | -0.10 | 0.31 |
| 325.1±9.5 | 0.22 | 0.67 | -0.02 | 0.26 |
| 448.0±1.4 | -0.15 | 0.40 | -0.02 | 0.08 |
| 448.0±3.0 | -0.17 | 0.57 | -0.13 | 0.28 |
| 448.0±7.2 | -0.05 | 0.66 | -0.23 | 0.46 |
| 664.0±4.2 | -0.07 | 0.91 | -0.49 | 0.76 |
| 874.4±6.0 | -0.12 | 1.02 | -0.65 | 0.90 |

lated observations produced with the polarized multistream radiative transfer model. Four testing databases are created: unpolarized brightness temperatures from clouds of bullet-rosettes calculated with the Eddington model and with the multistream model, and vertical and horizontal polarized brightness temperatures from clouds of columns calculated with the polarized multistream model. The testing databases are based on the same ice cloud and atmosphere statistics used in the previous sections. The CPU time to calculate the 10,000 cases in the tropical testing database is 36 sec for the Eddington model, 565 sec for the unpolarized multistream model, and 2225 sec for the polarized multistream computation. The retrievals are performed with the same two databases used before, which have clouds made of either 7-bullet rosettes or solid ice spheres, using set "C" of 12 microwave channels.

The results of this retrieval simulation are listed in Table 10. The IWP retrieval error for the Eddington model is lower here than in Table 7, presumably because this testing database consists only of bullet-rosette clouds and does not also contain clouds of solid ice spheres. The IWP retrieval accuracy for bullet-rosette clouds with the multistream model is comparable to that for the Eddington model (lower for the tropical simulation and higher for the midlatitude winter simulation). The retrieval accuracy for clouds of columns using vertically polarized brightness temperature is just slightly worse than for bullet-rosette clouds. The IWP retrieval accuracy for columns using horizontal polarization is much worse (median error averaged over the two simulations is 2.42 dB for horizontal vs. 1.04 dB for vertical polarization). Surprisingly, the $D_{me}$ retrieval error is lower for horizontal polarization. These retrieval simulation results for different particle shapes will, of course, depend on the assumptions made for the particle shapes in the retrieval database. Nevertheless, as expected from the forward modeling results in Evans et al. (1998), vertical polarization is much more robust to retrieval errors due to particle shape than is horizontal polarization. Based on this limited test, ice cloud retrieval errors due to oriented particles do not appear to be a significantly source of additional error to that modeled in the previous sections.

Table 10: Ice cloud retrieval accuracy from the particle shape/polarization tests.*

| | | | Tropical Simulation | | | | Midlatitude Winter Simulation | | | |
|---|---|---|---|---|---|---|---|---|---|---|
| | | | Median error | | | Ret | Median error | | | Ret |
| Model | Pol | Shape | IWP | $D_{me}$ | $Z_{med}$ | Frac | IWP | $D_{me}$ | $Z_{med}$ | Frac |
| Edd | none | rosette | 0.933 | 0.635 | 0.760 | 0.788 | 1.079 | 0.756 | 0.720 | 0.809 |
| MS1 | none | rosette | 0.881 | 0.651 | 0.770 | 0.788 | 1.116 | 0.782 | 0.750 | 0.820 |
| MS2 | V | column | 0.920 | 0.683 | 0.770 | 0.768 | 1.159 | 0.786 | 0.730 | 0.810 |
| MS2 | H | column | 2.095 | 0.628 | 0.710 | 0.698 | 2.745 | 0.524 | 0.680 | 0.706 |

*Median absolute error of ice water path (IWP), median mass equivalent sphere diameter ($D_{me}$), and height of median ice water path ($Z_{med}$) for cases with IWP above 2 g/m$^2$. "Ret Frac" is the fraction of the 10,000 retrievals that could be done without expanding the $\chi^2$ threshold. Model is "Edd" for the Eddington model, "MS1" is the multistream doubling-adding model with a single Stokes parameter, and "MS2" is the multistream model with two Stokes parameters. Pol is "none" for unpolarized brightness temperature, "V" for vertical polarization, and "H" for horizontal polarization. Shape gives the ice crystal shape assumed for all the clouds in the testing database. The 12 channel microwave set "C" was used in the retrievals.

## 8. Conclusions

Retrieval simulations have been carried out to determine the optimal microwave frequencies and infrared wavelengths of a conically scanning satellite instrument measuring the cloud properties ice water path (IWP), median equivalent sphere volume diameter ($D_{me}$), and median ice mass height ($Z_{medIWP}$). A total of 44 microwave frequencies from 183 to 916 GHz were grouped into 26 configurations, while 4 infrared wavelength bands were grouped into 6 configurations. Of the 26 microwave sets, 15 use six receivers, 2 use five receivers, 6 use four receivers, and 3 use three receivers. Many of the six channel configurations give similar retrieval accuracy, so which set has the lowest retrieval error is clearly dependent on the particular atmosphere and ice cloud statistics used in the two simulations (tropical anvil cloud and midlatitude winter synoptic cirrus). Furthermore, the Bayesian Monte Carlo integration retrieval technique adds its own uncertainty due to the finite number of cases in the retrieval database (even though $10^6$ cases were used).

General conclusions that may be drawn about the microwave frequencies are:

- Locating several receivers on water vapor lines above 183 GHz is better than using only window channels, though not overwhelmingly. Having all receivers centered on water vapor lines does not appear to be optimal because at the higher frequencies the wing channels have transmission that is too low compared to the window channels.

- When using receivers centered on water vapor lines, the range in offset frequencies should be as wide as possible, to give a large range in weighting function altitudes. It is most important to have the lowest possible altitude weighting functions (most transparent frequencies) in the channel set. This work was constrained by the desire to use an IF amplifier bandpass from 0.5 to 11 GHz, but channel sets with larger frequency offsets are desirable.

- Using oxygen lines does not work as well as using water vapor lines. This is perhaps due to the placement of the oxygen lines, but more likely due to their narrowness, which leads to smaller bandwidth and thus noisier channels.

- Receivers on oxygen lines do help somewhat with the water vapor retrievals, but good retrievals are only achieved with accurate layer temperatures provided by an NWP model.

- The exact placement of window channels, for example 220, 243, or 280 GHz and 643, 664, or 683 GHZ does not matter much. Some window frequencies might have better (lower altitude) weighting functions, but others may have more sensitivity to ice particles.

- Retrievals with four microwave receivers are almost as good as those with six receivers. Four receivers is clearly better than three receivers.

The infrared channels are a very important addition to the submillimeter channels for cirrus cloud retrievals. Using all four of the infrared channels studied does not seem to offer any benefit over three channels. The 6.7, 8.5, and 12.0 $\mu$m set of IR channels was slightly better than the 6.7, 11.0, and 12.0 $\mu$m set according to the simulations, but either could be used. Temperature profile information from NWP models, at least if accurate to the 1.5 K rms in 2 km thick layers assumed here, is extremely important for water vapor retrievals and also quite important for the median IWP cloud height retrievals.

The microwave channel configuration considered best in this study is set "C" with 12 channels at 183.31±1.5,3.5,7.0, 243.2±2.5, 325.15±1.5,3.5,9.5, 448.00±1.4,3.0,7.2, 664.0±4.2, and 874.4±6.0 GHz. In some ways set "I" with the 664 channel replaced by three channels at 620.7±0.9, 2.0, 7.5 GHz is better. A previous version of this study showed that the ice cloud retrievals were improved with four channels on the 448 GHz water vapor line (448.00± 0.8, 2.0, 4.5, 11.5 GHz), but the 11.5 GHz offset may not be technically feasible. A channel with an offset around 9.5 GHz is not effective because there is another (weaker) water vapor line at 439 GHz. The best candidate configuration with fewer receivers, and hence a cheaper instrument, appears to be set "S", which drops the 243 and 664 GHz receivers.

While the retrieval simulations in the channel selection study did include the effect of two extreme particle shapes (7-bullet rosettes and solid ice spheres), they did not consider the errors due to oriented particle shapes. A version of the ice cloud database generation code was developed that includes a fully polarized multistream radiative transfer model. This model was used to assess the accuracy of the much faster Eddington second approximation model normally used, which was found to have rms errors over all cases of 1.0 K at 874 GHz and less at lower frequencies. The polarized model was also used to show that the range in vertical - horizontal polarization brightness temperature difference due to horizontally oriented column ice crystals is much larger than that from randomly oriented bullet-rosettes. Retrieval simulations were performed using testing databases created with the polarized multistream model for clouds of horizontally oriented columns, but retrievals performed with the original unpolarized retrieval database (with sphere and rosette particle shapes). These retrievals showed that the IWP retrieval error is about the same as for randomly oriented particles when using vertical polarization, but much higher when using horizontal polarization. Therefore, it is recommended that vertical polarization be used for those microwave frequencies at which only one polarization is to be measured.

## 9. Acronym List

| | |
|---|---|
| ARM | Atmospheric Radiation Measurement |
| CEPEX | Central Equatorial Pacific Experiment |
| CIWSIR | Cloud Ice Water Sub-millimetre Imaging Radiometer |
| CoSSIR | Conical Scanning Submillimeter-wave Imaging Radiometer |
| CRYSTAL-FACE | Cirrus Regional Study of Tropical Anvils and Cirrus Layers - Florida Area Cirrus Experiment |
| FIRSC | Far Infrared Sensor for Cirrus |
| JPL | Jet Propulsion Laboratory |
| LBLRTM | Line-By-Line Radiative Transfer Model from Atmospheric and Environmental Research, Inc. |
| NASA | National Aeronautics and Space Administration |
| NWP | Numerical Weather Prediction |
| SWAS | Submillimeter Wave Astronomy Satellite |
| SWCIR | Submillimeter-Wave Cloud Ice Radiometer |
| IWC | ice water content (ice mass per volume) |
| IWP | ice water path (ice mass per area) |
| $D_{me}$ | median volume equivalent sphere particle diameter |
| $Z_{med}$ | median IWP cloud height |

## References


[1] Evans, K. F., and G. L. Stephens, 1991: A new polarized atmospheric radiative transfer model. *J. Quant. Spectrosc. Radiat. Transfer,* **46,** 413–423.

[2] Evans, K. F., S. J. Walter, A. J. Heymsfield and M. N. Deeter, 1998: Modeling of Submillimeter Passive Remote Sensing of Cirrus Clouds. *J. Appl. Met.,* **37,** 184–205.

[3] Evans, K. F., S. J. Walter, A. J. Heymsfield and G. M. McFarquhar, 2002: The Submillimeter-wave cloud ice radiometer: Simulations of retrieval algorithm performance. *J. Geophys. Res.,* 107(D3), 10.1029/2001JD000709.

[4] Heymsfield, A. J., S. Lewis, A. Bansemer, J. Iaquinta, L. M. Miloshevich, M. Kajikawa, C. Twohy, M. R. Poellot, 2002: A general approach for deriving the properties of cirrus and stratiform ice cloud particles. *J. Atmos. Sci.,* **59,** 3–29.

[5] McFarquhar, G. M., and A. J. Heymsfield, Microphysical characteristics of three anvils sampled during the central equatorial pacific experiment, *J. Atmos. Sci., 53*, 2401–2423, 1996.

[6] Miao, J., T. Rose, K. Kunzi, and P. Zimmermann, 2002: A future millimeter/sub-millimeter radiometer for satellite observation of ice clouds. *Int. J. Infrared Millimeter Waves,* **23,** 1159–1170.

[7] Vanek, M. D., I. G. Nolt, N. D. Tappan, P. A. R. Ade, F. Gannaway, C. Lee, P. A. Hamilton, K. F. Evans, J. Davis, S. Predko, 2001: Far InfraRed Sensor for Cirrus (FIRSC): An Aircraft-based FTS to Measure the Earth Radiance Spectrum. *Appl. Optics*, **40,** 2169–2176

[8] Yang, Ping, K. N. Liou, Klaus Wyser, David Mitchell, 2000: Parameterization of the scattering and absorption properties of individual ice crystals. *J. Geophys. Res.,* **105 (D4),** 4699–4718.